Structural basis for engagement by complement factor H of C3b on a self surface

Hugh P. Morgan[1,6], Christoph Q. Schmidt[2,6], Mara Guariento[2], Bärbel S. Blaum[2,5], Dominic Gillespie[1], Andrew P. Herbert[2,5], David Kavanagh[3], Haydyn D. T. Mertens[4], Dmitri I. Svergun[4], Conny M. Johansson[2] , Dušan Uhrín[2], Paul N. Barlow[2] & Jonathan P. Hannan[1]

[1]Institute of Structural and Molecular Biology, School of Biological Sciences, King's Buildings, Mayfield Road, University of Edinburgh, Edinburgh, EH9 3JR, UK.

[2]Edinburgh Biomolecular NMR Unit, EaStCHEM, School of Chemistry, University of Edinburgh, Edinburgh, EH9 3JJ, UK.

[3]The Institute of Human Genetics, University of Newcastle upon Tyne, NE1 3BZ, UK

[4]European Molecular Biology Laboratory, Hamburg Outstation, Notkestraße 85, D-22603 Hamburg, Germany

[5]Present address: Interfaculty Institute for Biochemistry, University of Tübingen, D-72076 Tübingen, Germany (B.S.B); The Physiological Laboratory, School of Biomedical Sciences, Crown Street, University of Liverpool, Liverpool, L69 3BX, UK (A.P.H).

[6]Denotes each author contributed equally to this study

Correspondence should be addressed to P.N.B (Paul.Barlow@ed.ac.uk) or J.P.H. (Jonathan.Hannan@ed.ac.uk).

SUPPLEMENTARY MATERIAL

Supplementary Tables 1 Macromolecular interfaces observed in the C3d:FH19–20 complex structure (the physiological B-F/A-E interface).

Supplementary Tables 2 Macromolecular interfaces observed in the C3d:FH19–20 complex structure (the non-physiological A-D interface).

Supplementary Table 3 SPR steady state binding affinities of FH fragments for C3d variants.

Supplementary Figure 1 The C3d:FH19–20 interface at pH 7.0 and 9.0.

Supplementary Figure 2 Supplementary Figure 2 C3d:FH19–20 crystal interfaces extrapolated onto the C3b:FH1–4 complex**.**

Supplementary Figure 3 [^{1}H,^{15}N]-HSQC spectra of the C3d:FH19–20 complex, the GAG titration of ^{15}N-FH19–20, and the GAG titration of the C3d:FH19–20 complex.

Supplementary Figure 4 Surface plasmon resonance analysis of the C3d/C3dg/C3b:FH interaction.

Supplementary Figure 5 Erythrocyte hemolysis assay.

Suppmentary Figure 6 GST-C3d:dp8 competition assay

Supplementary Figure 7 SAXS data and *ab initio* modelling.

Supplementary Figure 8 Efb-C:C3d binding.

Supplementary Figure 9 C3d and FH19–20 sequence alignments.

Supplementary Methods

Supplementary References

(a)

C3d	FH	Symmetry op-n	Interface area (Å²)	Interface hydrogen bonds
A	D	x, y, z	863.7	5
B	F	x, y, z	749.9	12
A	E	x, y-1, z	715.9	12
C	D	x, y, z	625.9	3
B	D	x, y, z	572.3	5
C	E	x-1,y,z	359.6	5
B	E	x,y,z	333.8	3
A	F	x,y-1,z-1	239.9	3

(b)

Interaction	**FH chain/residue**	**Distance (Å)**	**C3d chain residue**
1	F:GLN1139[NE2]	2.93	B:GLN 119[OE1]
2	F:GLN1139[NE2]	2.99	B:ILE 115[O]
3	F:ASN1140[N]	3.31	B:LEU 116[O]
4	F:TYR1190[OH]	2.62	B:ASP 122[OD1]
5	F:ASN1117[OD1]	2.84	B:LYS 178[NZ]
6	F:GLN1139[OE1]	2.92	B:LYS 178[NZ]
7	F:TYR1142[OH]	3.06	B:LYS 178[NZ]
8	F:ASP1119[OD2]	3.47	B:SER 171[OG]
9	F:ASP1119[OD2]	3.15	B:ASN 170[N]
10	F:ASP1119[OD2]	3.15	B:SER 171[N]
11	F:ILE1120[O]	2.90	B:LYS 112[NZ]
12	F:SER1122[O]	3.05	B:LYS 112[NZ]
Equivalent interactions formed with a symmetry related FH molecule.			
1a	E:GLN1139[NE2]	2.93	A:GLN 119[OE1]
2a	E:GLN1139[NE2]	3.10	A:ILE 115[O]
3a	E:ASN1140[N]	3.20	A:LEU 116[O]
4a	E:TYR1190[OH]	3.17	A:ASP 122[N]
5a	E:ASN1117[OD1	2.77	A:LYS 178[NZ]
6a	E:GLN1139[OE1]	2.88	A:LYS 178[NZ]
7a	E:TYR1142[OH]	2.92	A:LYS 178[NZ]
8a	E:ASP1119[OD2]	2.76	A:SER 171[OG]
9a	E:ASP1119[OD2]	3.37	A:ASN 170[N]
10a	E:ASP1119[OD2]	3.16	A:SER 171[N]
11a	E:ILE1120[O]	2.81	A:LYS 112[NZ]
12a	E:SER1122[O]	3.01	A:LYS 112[NZ]

Hydrogen bond = ≤ 3.5Å

(**c**)

Interaction	FH chain/residue	Distance (Å)	C3d chain residue
1	F:PRO 1166 [CG]	3.46	B:PRO 121[CG]
2	F:PRO 1166 [CG]	3.52	B:PRO 121[CB]
3	F:LEU 1141[CB]	3.94	B:PRO 121[CG]
4	F:LEU 1141[CD1]	3.68	B:PRO 121[CG]
5	F:LEU 1141[CD1]	3.72	B:PRO 121[CD]
6	*F:TYR 1190	-	B:PRO 121
Equivalent interactions formed at a symmetry related interface.			
1	F:PRO 1166[CG]	3.47	B:PRO 121[CG]
2	F:PRO 1166[CG]	3.59	B:PRO 121[CB]
3	F:LEU 1141[CB]	4.05	B:PRO 121[CG]
4	F:LEU 1141[CD1]	3.87	B:PRO 121[CG]
5	F:LEU 1141[CD1]	3.99	B:PRO 121[CD]
6	*F:TYR 1190	-	B:PRO 121

Hydrophobic interaction = 3.4 – 4.2 Å

Supplementary Tables 1 (**a**) Macromolecular interfaces observed in the C3d:FH19–20 complex structure. Hydrogen bond = ≤ 3.5Å; Red = Likely C3d:FH19–20 physiologically relevant interfaces. Chains B-F and A-E (Chain E and symmetry related chain A) form highly conserved interfaces. (**b**) (B-F/A-E interface) Hydrogen bonds formed between C3d and FH19–20 molecules. (**c**) (B-F/A-E interface) Potential hydrophobic interactions formed between C3d and FH molecules. *The Pro1166-Pro121 (C3 prepro numbering: P1114) stacking interaction is sandwiched between the phenol rings of Tyr1142-Tyr1190 and between Val1168-Leu1141 creating an extremely hydrophobic environment. All molecular interfaces were analyzed using the program PISA [1].

(**a**)

Interaction	FH chain/residue	Distance (Å)	C3d chain residue
1	D:TYR1177[OH]	2.74	A:THR 13[O]
2	D:THR1227[OG1]	3.03	A:SER 15[OG]
3	D:ARG1210[O]	3.22	A:SER 15[OG]
4	D:ARG1210[O]	2.87	A:GLY 16[N]
5	D:CYS1228[O]	2.84	A:GLN 20[NE2]

Hydrogen bond = ≤ 3.5Å

(**b**)

Interaction	FH chain/residue	Distance (Å)	C3d chain residue
1	D:ILE 1173[CD1]	3.77	A:VAL 12[CG1]
2	D:ILE 1173[CG2]	3.70	A:VAL 12[CG1]

Hydrophobic interaction = 3.4 – 4.2 Å

Supplementary Tables 2 (**a**) (A-D interface) Hydrogen bonds formed between C3d and FH molecules. It should be noted that R1210C (aHUS-associated) and R1210S (designed) forms of FH19–20 do not exhibit significantly altered binding with C3b [2], and in this study the R1210C mutant did not demonstrate decreased binding to C3dg or C3d (Supplementary Table 6). (**b**) (A-D interface) Potential hydrophobic interactions between C3d and FH molecules.

	SPR binding affinity [μM]							
FH fragments	Recombinant C3d	Plasma C3d	C3dg	C3d E117A	C3d D122A	C3d E117A/ D122A	C3d E160A	C3d I164A
15–18	n.d.	n.d.	n.d.	-	-	-	-	-
15–19	n.d.	n.d.	n.d.	-	-	-	-	-
18–20	8.8±0.6	9.7±0.6	3.8±0.2	-	-	-	-	-
19–20 wt	6.2±0.4	8.2±0.6	3.8±0.5	*34±1	*46±5	*29.8 x 10^3± 1.6 X 10^3†	15±2	14.0 ± 1.4†
19–20 wt + 20 fold excess of Fondaparinux	13.7±0.3 †	-	-	-	-	-	-	-
19–20 D1119G	n.d.	n.d.	n.d.	-	-	-	-	-
19–20 R1182S	11.2±0.4	13.8±0.4	8.1±0.2	*51±3	*55±6	-	26±0.4	-
19–20 W1183L	6.6±0.2	8.2±0.3	5.3±0.2	-	-	-	-	-
19–20 W1183R	2.9±0.2	4.9±0.4	1.9±0.1	-	-	-	-	-
19–20 T1184R	4.2±0.1	6.8±0.2	4.4±0.2	-	-	-	-	-
19–20 L1189F	5.3±0.6	6.3±0.7	2.1±0.6	*28±1	*46±5	-	14±0.3	-
19–20 L1189R	1.8±0.04	2.4±0.06	1.3±0.1	11±0.4	*29±1.5		4.6±0.1	
19–20 S1191L	3.9±0.2	4.6±0.2	1.8±0.2	-	-	-	-	-
19–20 V1197A	5.7±0.5	10.1±0.8	4.4±0.3	-	-	-	-	-
19–20 S1191L V1197A	4.6±0.2	5.2±0.2	1.9±0.2	-	-	-	-	-
19–20 R1203S	11.4±0.4	13.7±0.3	11.5±0.3	-	-	-	-	-
19–20 R1210C	6.2±0.3	5.3±0.2	2.4±0.1	-	-	-	-	-
19–20 R1215Q	11.0±0.5	13.1±0.6	8.0±0.1	*41±2	*48±4.2	-	*21±2	-

Supplementary Table 3 SPR steady state binding affinities of FH fragments for C3d variants used in this study. C3dg was immobilized via the thioester, while all other C3d entities were amine-coupled (see **Supplementary Methods**). * denotes an extrapolated K_D value which lies outside the concentration range assayed. n.d., non detectable. A dash indicates that the corresponding proteins were not assayed. † denotes K_D values were measured on a separate chip to the other C3d mutations. On this occasion the K_D value for wild-type C3d (in a different flow-cell on the same chip was recorded at ~17.6 μM ± 0.8 μM).

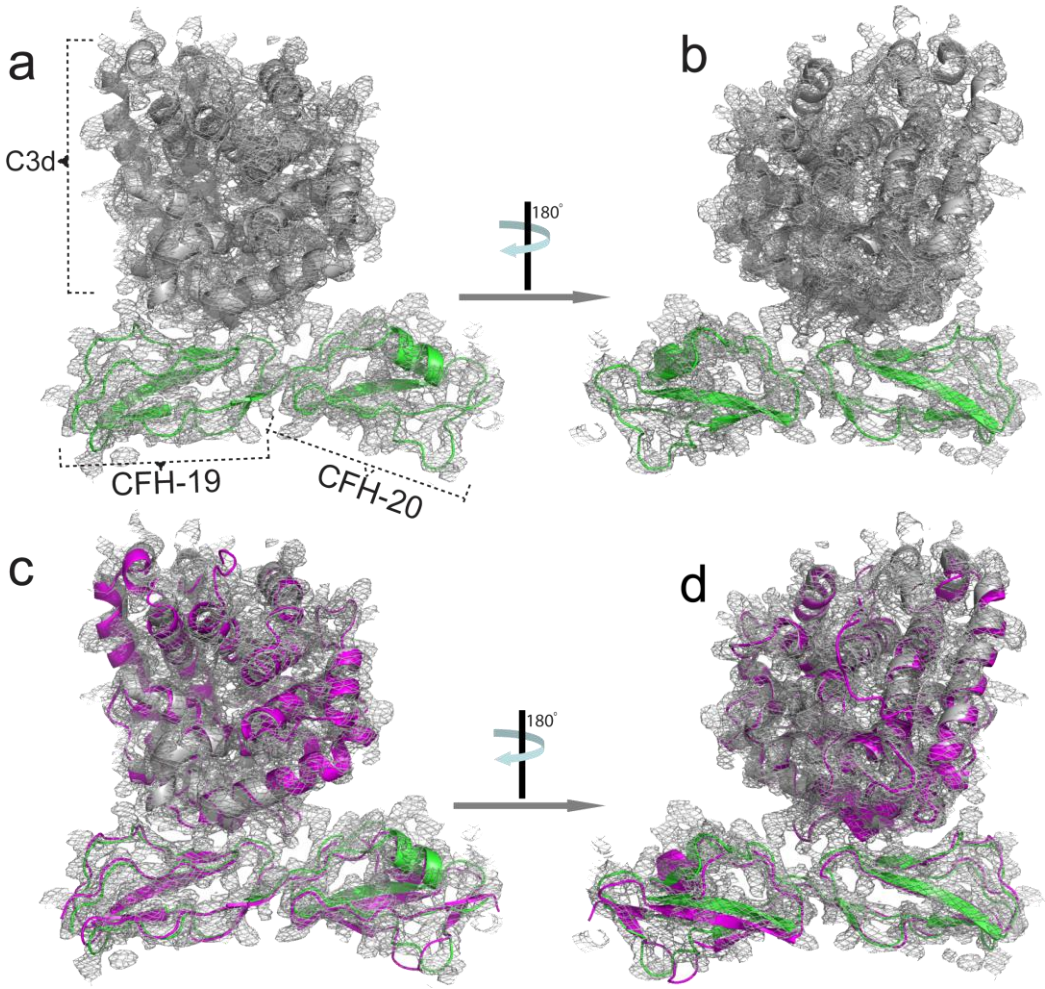
a
C3d
CFH-19
CFH-20
180°
b
c
180°
d

e

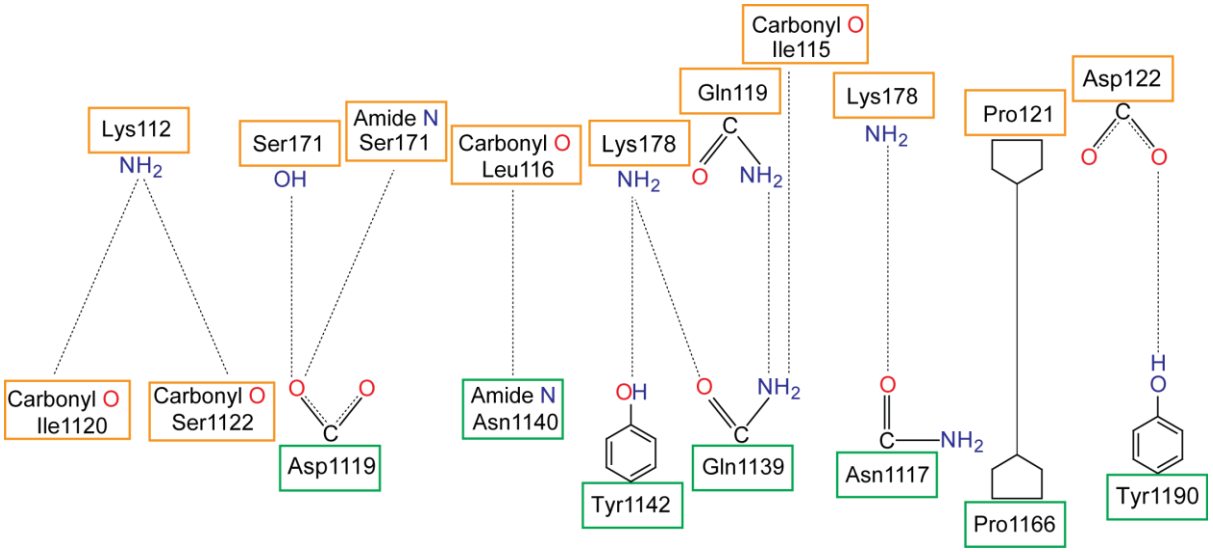
Lys112
NH2
Carbonyl O
Ile1120
Carbonyl O
Ser1122
Ser171
OH
Amide N
Ser171
Asp1119
Carbonyl O
Leu116
Amide N
Asn1140
Lys178
NH2
Tyr1142
Gln119
Carbonyl O
Ile115
Gln1139
Lys178
NH2
Asn1117
Pro121
Pro1166
Asp122
Tyr1190

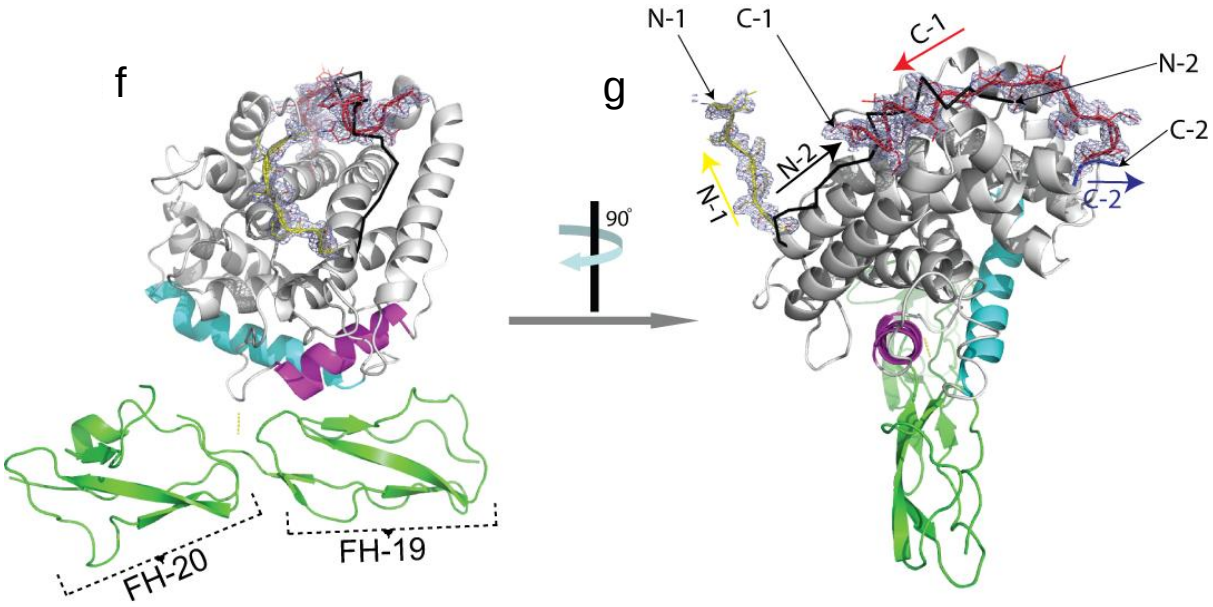

Supplementary Figure 1 (a-d) The C3d:FH19–20 complex interface is conserved at both pH 7.0 and 9.0. (**a-b**) Two views of a C3d:FH19–20 complex crystallized at pH 7. Each monomer has been colored to aid identification. The pH 7.0 C3d:FH19–20 complex is shown with its complete electron density ($2F_o$-F_c map). The resolution of the map is 3.5 Å and is contoured at 1.0σ. (**c-d**) Two views of the superposed C3d:FH19–20 structures, crystallized at pH 9.0 (magenta) and pH 7.0 (green and grey). (**e**) A schematic representation of the C3d:FH19–20 interface at pH 9.0. (**f, g**) Two orthogonal views of the C3d:FH19–20 complex superposed onto the remaining two C3d chains, which make up the asymmetric unit. C3d monomers had an average RMSD of 0.33 (range 0.44-0.26Å) for all Cα atoms of residues 18–294. For clarity only the N- and C-termini are shown, as these areas exhibited the greatest RMS difference. The different positions of the C- (C-1 – yellow ribbon) and N-termini (N-1 – red ribbon) of C3d belonging C3d:FH19–20 complex, compared to the C- (C-2 – blue ribbon) and N-termini (N-2 – black ribbon) of the two C3d chains observed in the asymmetric unit of the crystal structure. Arrows have been added to illustrate the different directions observed for the backbones of the N- and C-termini.

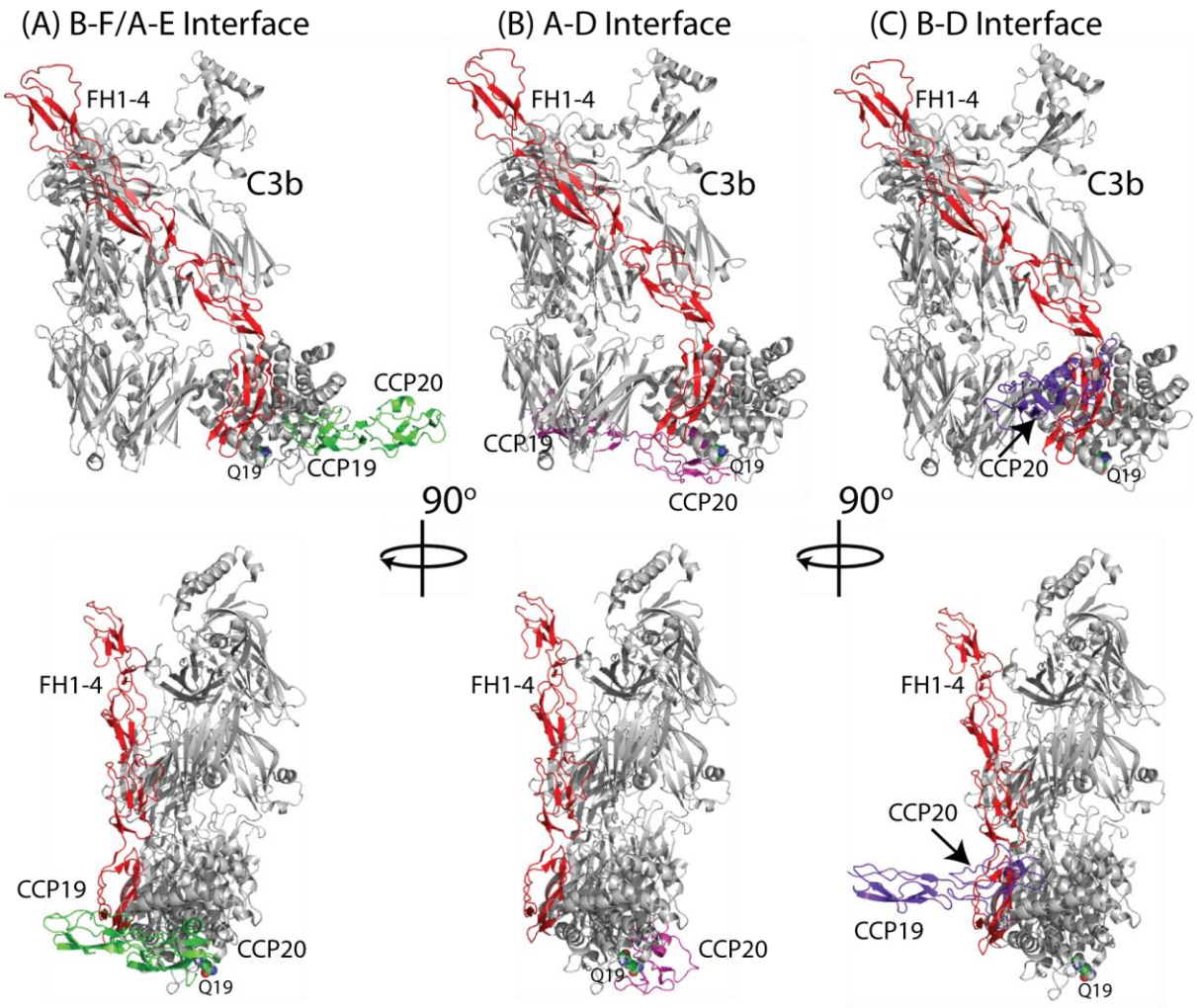

Supplementary Figure 2 C3d:FH19–20 crystal interfaces extrapolated onto the C3b:FH1–4 complex (PDB accession code: 1WII, [3]) shown in two different orientations. (**A**) B-F and symmetry related A-E interface; (**B**) A-D interface; and (**C**) the B-D interface. The B-F/A-E interface was selected to represent the physiological C3b:FH19–20 interaction for the following reasons: (i) No steric clashes were observed in the context of the larger C3b:FH1-4:FH19–20 complex. (ii) In the B-F/A-E interface no overlap occurs between the site of FH19–20 binding and the site of covalent attachment of C3d/TED to biological surfaces, centered around residue Gln19 (pre-pro C3 numbering Gln1013). (iii) The B-F/A-E interface is characterized by more extensive hydrogen-bonding and hydrophobic interactions than those of either the A-D or B-D interfaces, and is highly conserved in mammalian orthologues (Supplementary Tables 1-2 and

Supplementary Fig. 9). (iv) By NMR the greatest line-broadening observed upon addition of C3d to ^{15}[N]-labeled FH was for resonances corresponding to residues within the B-F/A-E interface, but not those within the A-D or B-D interfaces (Fig. 3 and Supplementary Fig. 3b). (v) Mutation of FH residues Asp1119 (D1119G) and Gln1139 (Q1139A); and C3d residues Glu117 (E117A; E1110A), Asp122 (D122A; D1115A) and Glu117 Asp122 (E117A D122A; E1110A D1115A), within the B-F/A-E interface results in altered C3b:FH19–20 or C3d:FH19–20 binding ([2,4]; Supplementary Table 3 and Fig. 4, Supplementary Fig. 4) (vi) The A-D interface involves a surface of C3d/TED that is unavailable for binding in the context of C3b according to the crystal structures of C3b [5], C3b complexed with FH:1-4 [3] and C3b complexed with CRIg [6]; (vii) The A-D interface would also unavailable to FH19–20 under physiologic conditions due to overlap with the site of covalent attachment to biological surfaces; (viii) Mutation of residue Arg1210 (aHUS-associated R1210C or designed R1210S) which is involved in a number of hydrogen bonds within the A-D interface has little effect on C3d/C3b binding ([2]; Supplementary Table 3 and Supplementary Fig. 4). Furthermore, Arg1210 is not conserved in other mammalian orthologues of FH (Supplementary Figure 9); (ix) The B-D interface clashes with the FH CCP4 binding site [3], and also overlaps with the Efb-C binding surface [7]. But Efb-C enhances FH binding to C3b and C3d [8]; (x) Mutation of C3d residues directed towards the B-D interface, E160A (E1153A) and I164A (I1157A) result in little or no decrease in FH binding (Supplementary Fig. 4).

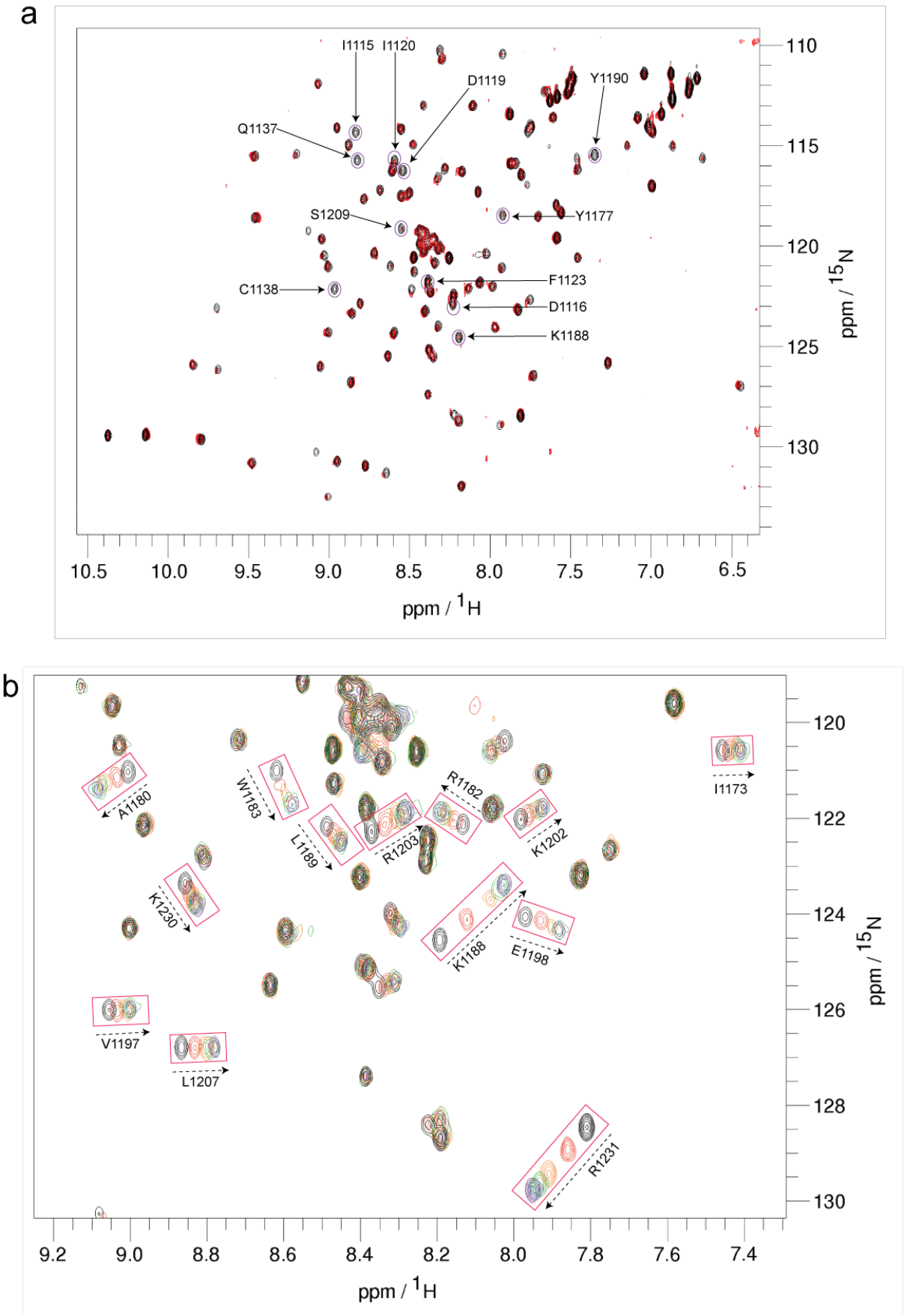
a
I1115
I1120
D1119
Y1190
Q1137
S1209
Y1177
F1123
C1138
D1116
K1188
110
115
120
125
130
ppm / 15N
10.5
10.0
9.5
9.0
8.5
8.0
7.5
7.0
6.5
ppm / 1H
b
A1180
W1183
L1189
R1182
R1203
K1202
I1173
K1230
K1188
E1198
V1197
L1207
R1231
120
122
124
126
128
130
ppm / 15N
9.2
9.0
8.8
8.6
8.4
8.2
8.0
7.8
7.6
7.4
ppm / 1H

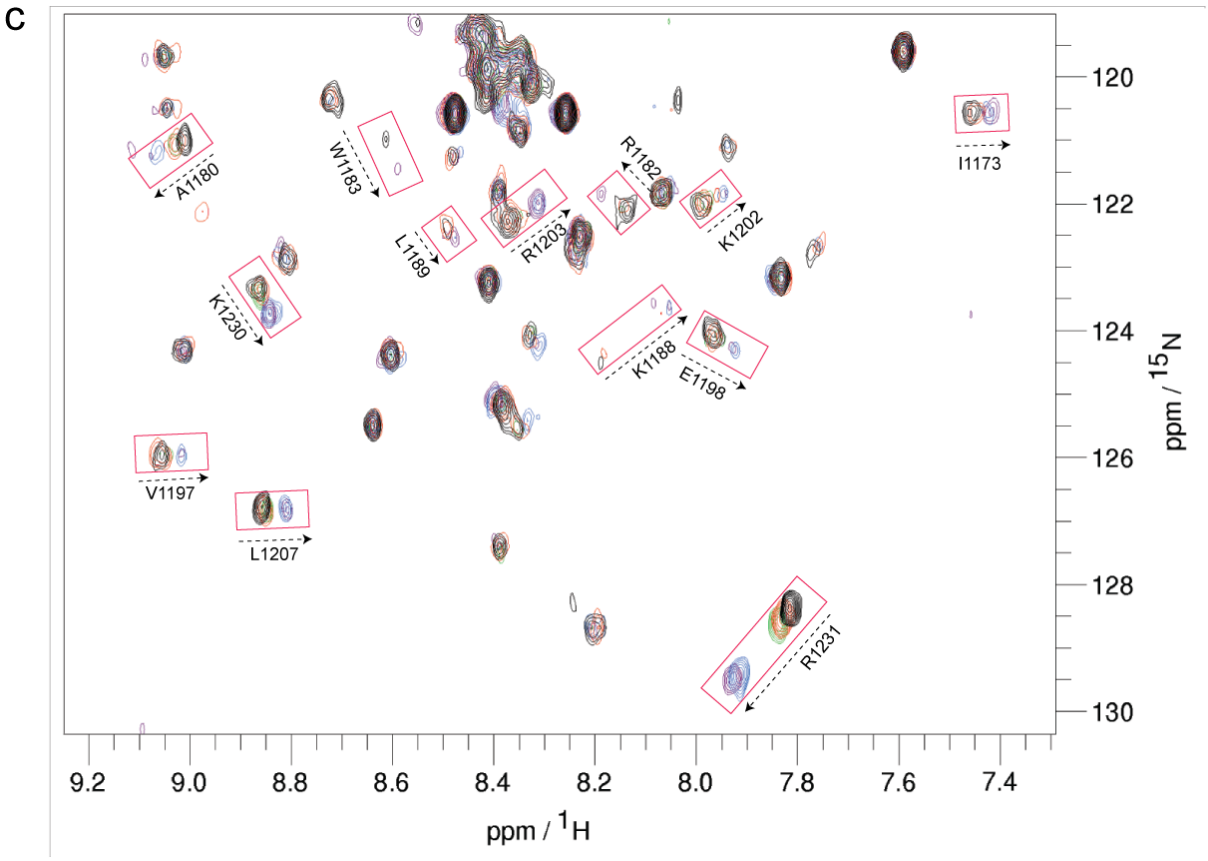

Supplementary Figure 3 (**a**) Overlay of [^{1}H,^{15}N]-HSQC spectra of free ^{15}N-FH19–20 (black) and in the presence of 1.6 molar access of unlabeled C3d (red). The starting contour level for the black spectrum was set higher in order to compensate for the large signal loss in the presence of C3d. Labels highlight cross peaks which experienced a >90% loss in intensity (indicated in red on the structure of FH19–20; Fig. 3b). (**b**) Overlay of partial [^{1}H,^{15}N]-HSQC spectra of FH19–20 after addition of heparin octasaccharide, dp8. Protein : ligand ratios are 1:0 (black), 1:0.5 (red), 1:1.1 (orange), 1:2.1 (green), 1:4.3 (blue) and 1:8.5 (purple). (**c**) Overlay of partial [^{1}H,^{15}N]-HSQC spectra of ^{15}N-FH19–20:C3d (1:1.6) complex after addition of dp8. Protein : ligand ratios are 1:0 (black), 1:0.3 (red), 1:0.6 (green) 1:7.9 (blue) and 1:15.0 (purple).

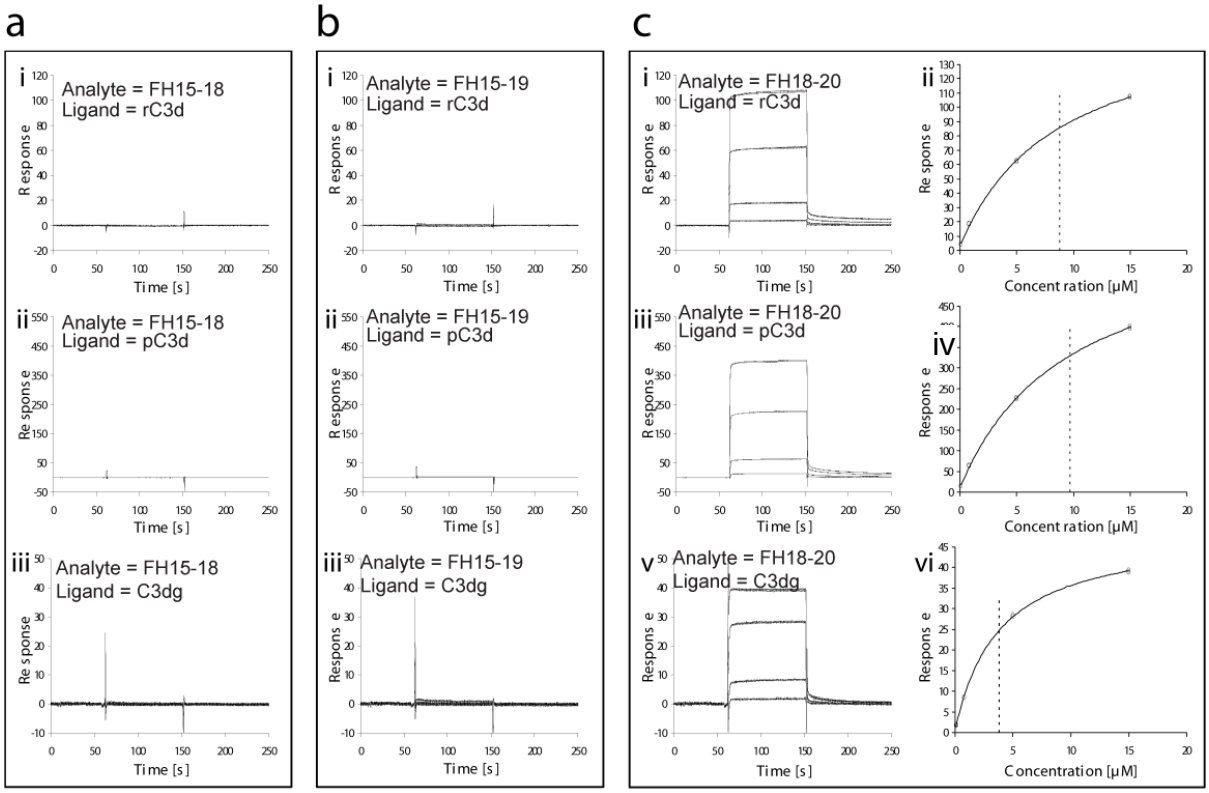
a
i
Analyte = FH15-18
Ligand = rC3d
ii
Analyte = FH15-18
Ligand = pC3d
iii
Analyte = FH15-18
Ligand = C3dg
b
i
Analyte = FH15-19
Ligand = rC3d
ii
Analyte = FH15-19
Ligand = pC3d
iii
Analyte = FH15-19
Ligand = C3dg
c
i
Analyte = FH18-20
Ligand = rC3d
ii
iii
Analyte = FH18-20
Ligand = pC3d
iv
v
Analyte = FH18-20
Ligand = C3dg
vi
Time [s]
Concentration [µM]

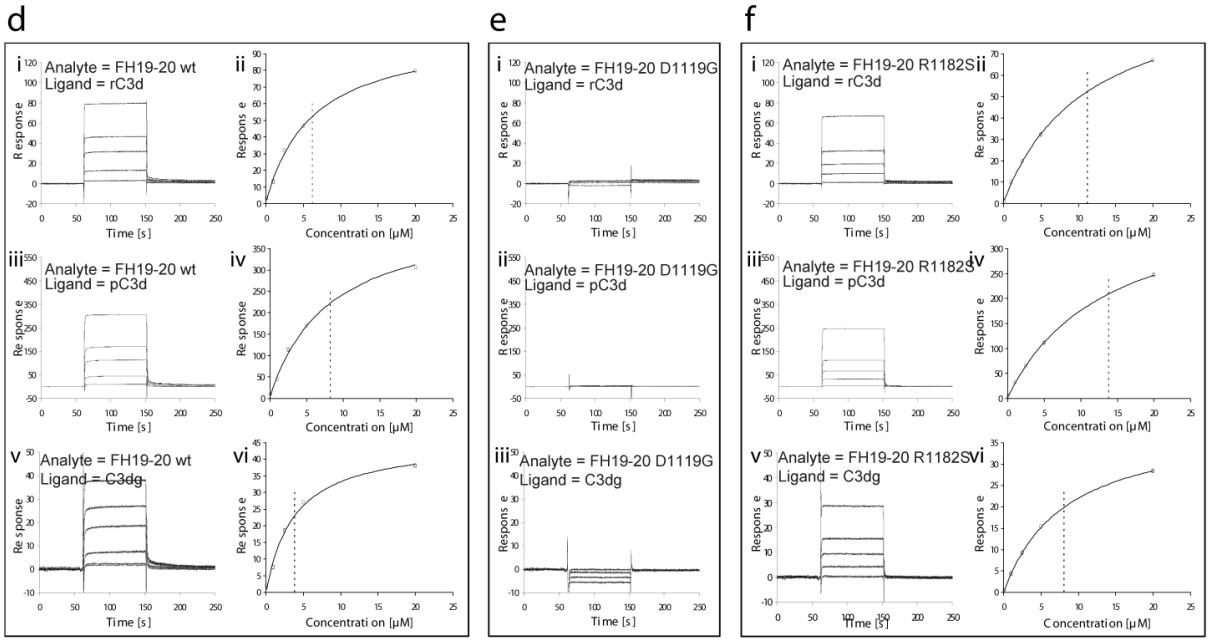
d
i
Analyte = FH19-20 wt
Ligand = rC3d
ii
iii
Analyte = FH19-20 wt
Ligand = pC3d
iv
v
Analyte = FH19-20 wt
Ligand = C3dg
vi
e
i
Analyte = FH19-20 D1119G
Ligand = rC3d
ii
Analyte = FH19-20 D1119G
Ligand = pC3d
iii
Analyte = FH19-20 D1119G
Ligand = C3dg
f
i
Analyte = FH19-20 R1182S
Ligand = rC3d
ii
iii
Analyte = FH19-20 R1182S
Ligand = pC3d
iv
v
Analyte = FH19-20 R1182S
Ligand = C3dg
vi
Time [s]
Concentrati on [µM]
Concentration [µM]

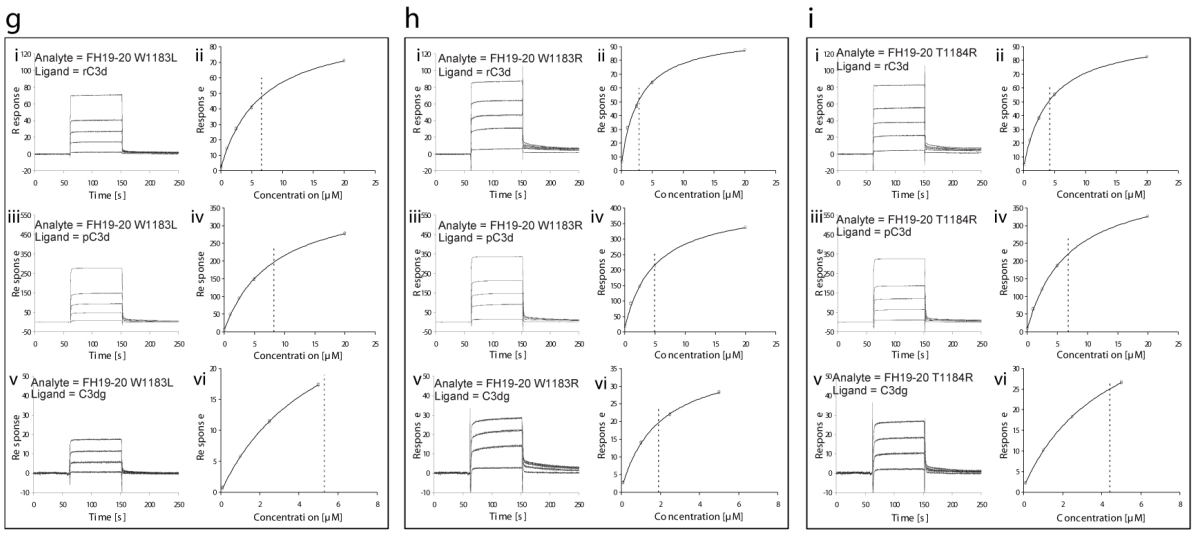
g
i
Analyte = FH19-20 W1183L
Ligand = rC3d
ii
iii
Analyte = FH19-20 W1183L
Ligand = pC3d
iv
v
Analyte = FH19-20 W1183L
Ligand = C3dg
vi
h
Analyte = FH19-20 W1183R
Ligand = rC3d
Analyte = FH19-20 W1183R
Ligand = pC3d
Analyte = FH19-20 W1183R
Ligand = C3dg
i
Analyte = FH19-20 T1184R
Ligand = rC3d
Analyte = FH19-20 T1184R
Ligand = pC3d
Analyte = FH19-20 T1184R
Ligand = C3dg
Time [s]
Concentration [µM]

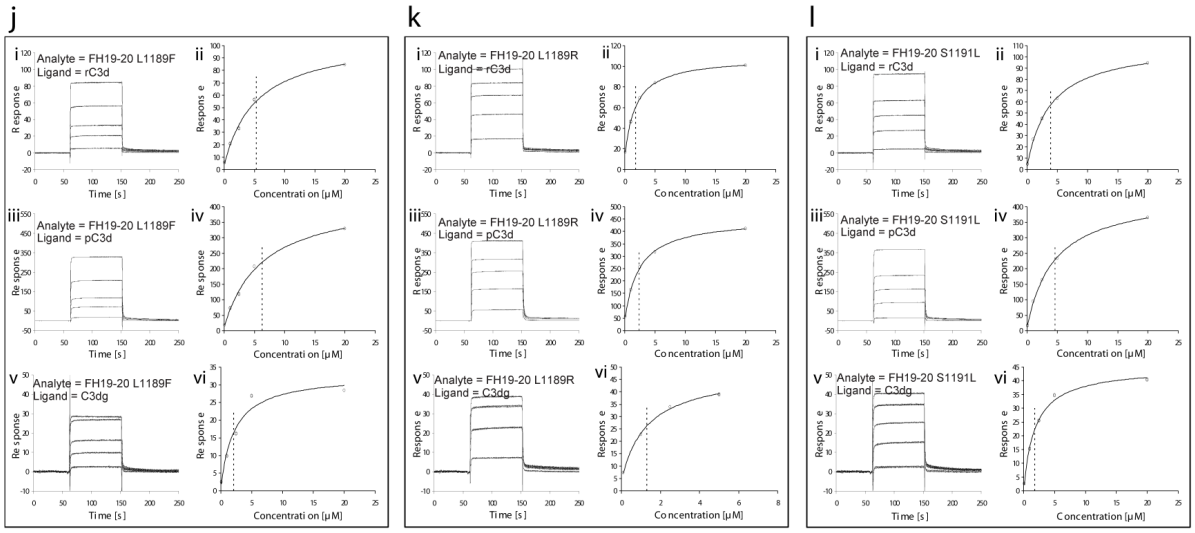
j
i
Analyte = FH19-20 L1189F
Ligand = rC3d
ii
iii
Analyte = FH19-20 L1189F
Ligand = pC3d
iv
v
Analyte = FH19-20 L1189F
Ligand = C3dg
vi
k
Analyte = FH19-20 L1189R
Ligand = rC3d
Analyte = FH19-20 L1189R
Ligand = pC3d
Analyte = FH19-20 L1189R
Ligand = C3dg
l
Analyte = FH19-20 S1191L
Ligand = rC3d
Analyte = FH19-20 S1191L
Ligand = pC3d
Analyte = FH19-20 S1191L
Ligand = C3dg
Time [s]
Concentration [µM]

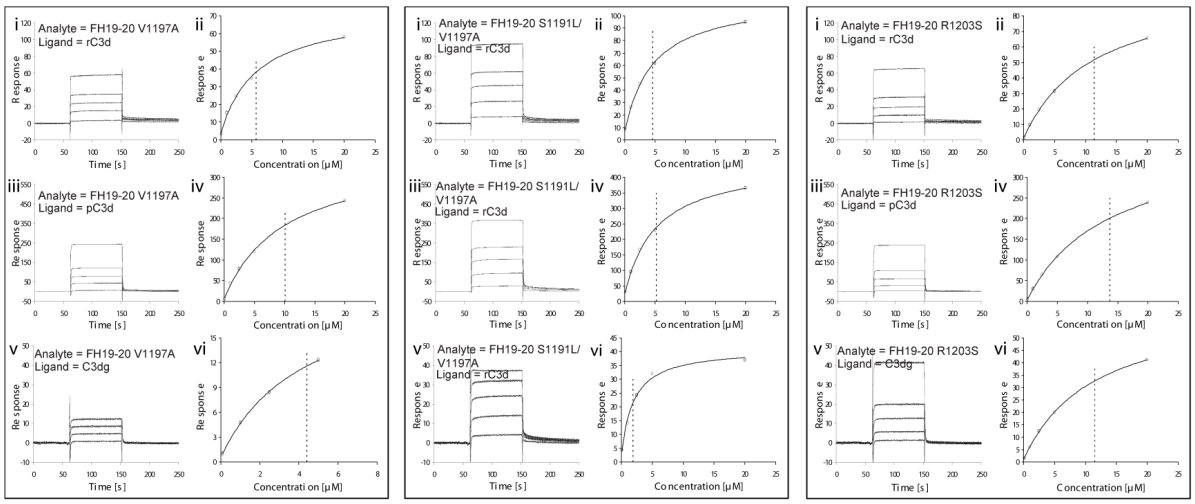
m
i
Analyte = FH19-20 V1197A
Ligand = rC3d
ii
iii
Analyte = FH19-20 V1197A
Ligand = pC3d
iv
v
Analyte = FH19-20 V1197A
Ligand = C3dg
vi
n
Analyte = FH19-20 S1191L/
V1197A
Ligand = rC3d
Analyte = FH19-20 S1191L/
V1197A
Ligand = rC3d
Analyte = FH19-20 S1191L/
V1197A
Ligand = rC3d
o
Analyte = FH19-20 R1203S
Ligand = rC3d
Analyte = FH19-20 R1203S
Ligand = pC3d
Analyte = FH19-20 R1203S
Ligand = C3dg
Time [s]
Concentration [µM]

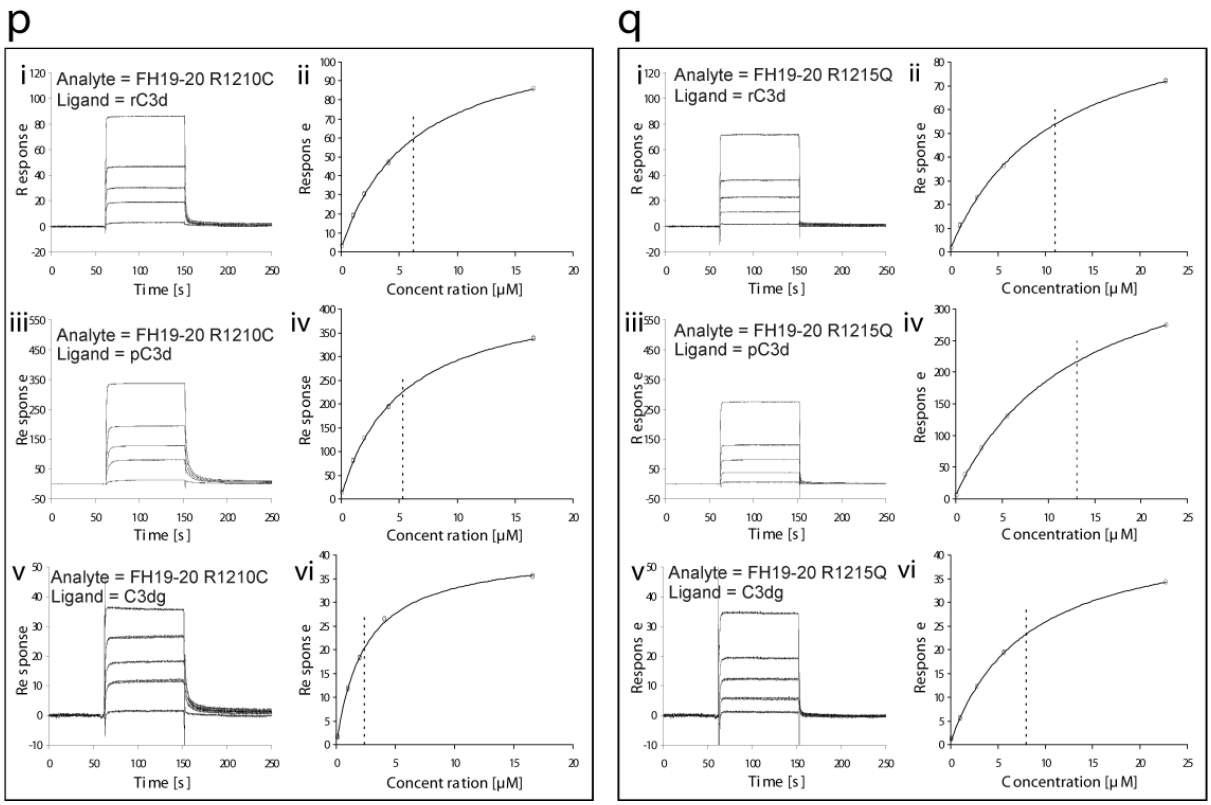
p
i
Analyte = FH19-20 R1210C
Ligand = rC3d
Response
Time [s]
ii
Concentration [µM]
iii
Analyte = FH19-20 R1210C
Ligand = pC3d
iv
v
Analyte = FH19-20 R1210C
Ligand = C3dg
vi
q
Analyte = FH19-20 R1215Q
Ligand = rC3d
Analyte = FH19-20 R1215Q
Ligand = pC3d
Analyte = FH19-20 R1215Q
Ligand = C3dg

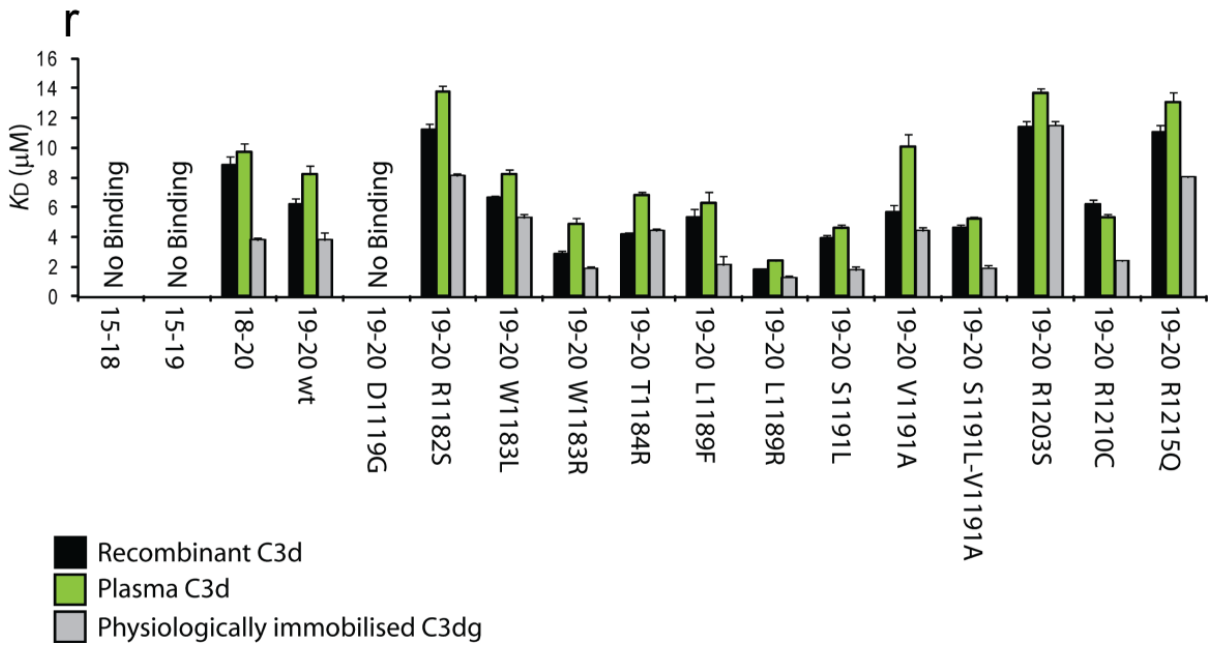
r
KD (µM)
No Binding
No Binding
No Binding
15-18
15-19
18-20
19-20 wt
19-20 D1119G
19-20 R1182S
19-20 W1183L
19-20 W1183R
19-20 T1184R
19-20 L1189F
19-20 L1189R
19-20 S1191L
19-20 V1191A
19-20 S1191L-V1191A
19-20 R1203S
19-20 R1210C
19-20 R1215Q
Recombinant C3d
Plasma C3d
Physiologically immobilised C3dg

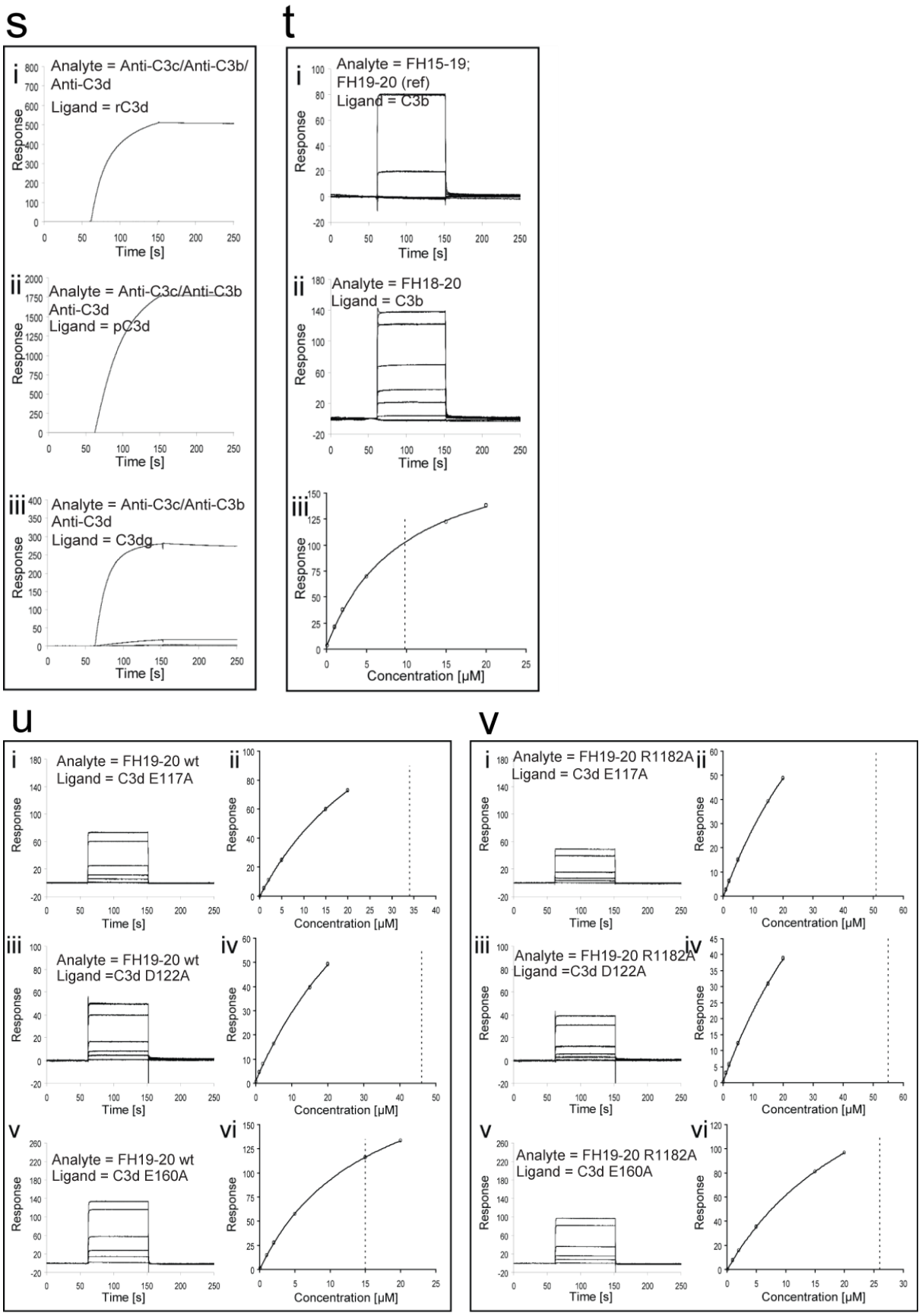
s
i
Analyte = Anti-C3c/Anti-C3b/
Anti-C3d
Ligand = rC3d
Response
Time [s]
ii
Analyte = Anti-C3c/Anti-C3b
Anti-C3d
Ligand = pC3d
Response
Time [s]
iii
Analyte = Anti-C3c/Anti-C3b
Anti-C3d
Ligand = C3dg
Response
Time [s]
t
i
Analyte = FH15-19;
FH19-20 (ref)
Ligand = C3b
Response
Time [s]
ii
Analyte = FH18-20
Ligand = C3b
Response
Time [s]
iii
Response
Concentration [μM]
u
i
Analyte = FH19-20 wt
Ligand = C3d E117A
Response
Time [s]
ii
Response
Concentration [μM]
iii
Analyte = FH19-20 wt
Ligand =C3d D122A
Response
Time [s]
iv
Response
Concentration [μM]
v
Analyte = FH19-20 wt
Ligand = C3d E160A
Response
Time [s]
vi
Response
Concentration [μM]
v
i
Analyte = FH19-20 R1182A
Ligand = C3d E117A
Response
Time [s]
ii
Response
Concentration [μM]
iii
Analyte = FH19-20 R1182A
Ligand =C3d D122A
Response
Time [s]
iv
Response
Concentration [μM]
v
Analyte = FH19-20 R1182A
Ligand = C3d E160A
Response
Time [s]
vi
Response
Concentration [μM]

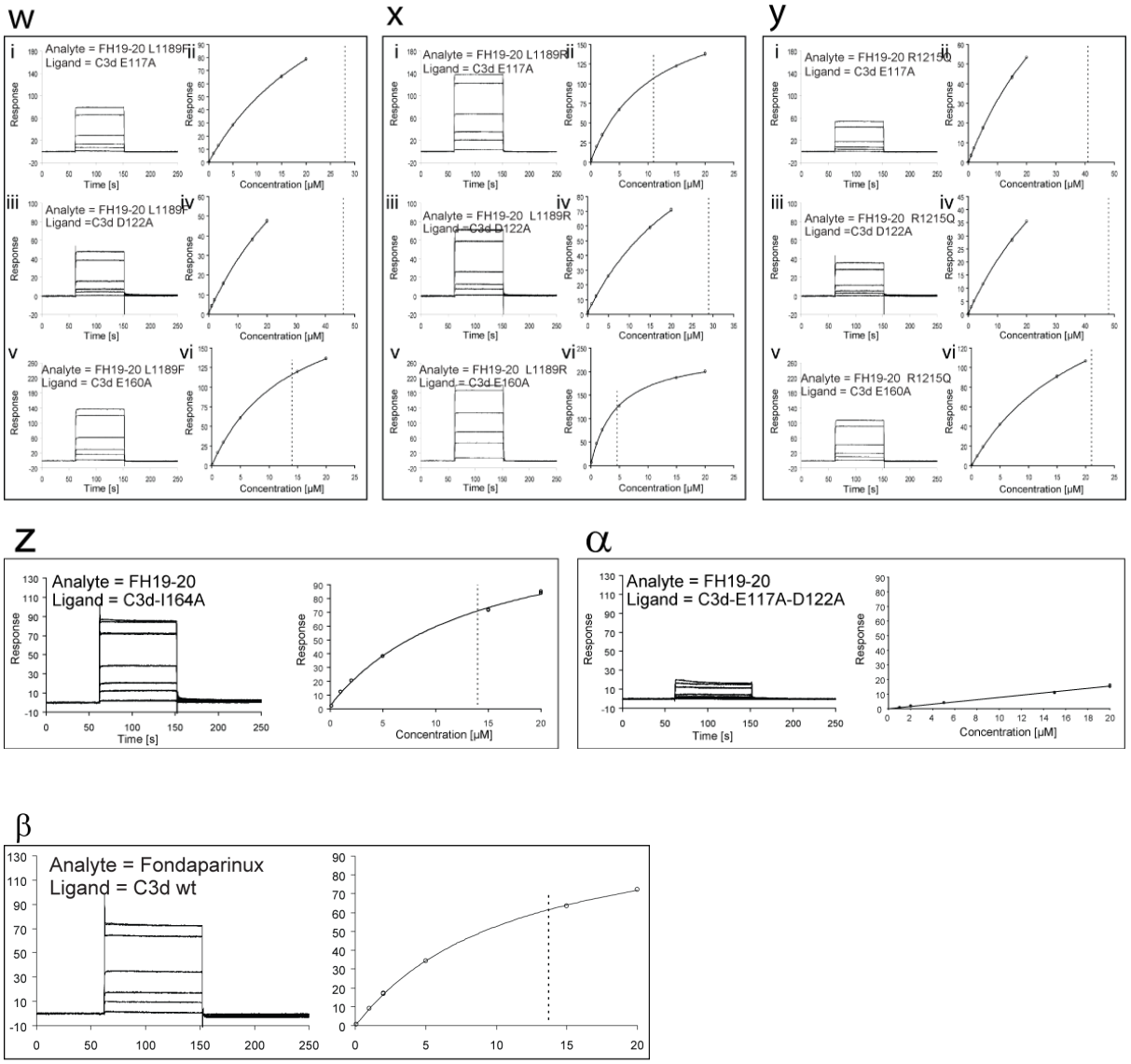

Supplementary Figure 4 Surface plasmon resonance analysis of the C3d/C3dg/C3b:FH interaction. Analytes and ligands are indicated in the panels. Analytes were injected in variable concentrations from 0.1 μM up to 5, 15 or 20 μM. All analyte injections were carried out in duplicate and duplicate sensorgrams of reference-surface subtracted responses are plotted. Where binding was detected sensorgrams and corresponding K_D fitting are shown on the left and right, respectively. For non-binders, only the sensorgrams are shown. Dissociation constants were calculated by fitting steady-state binding levels derived from the background-subtracted traces to a one-to-one binding

steady-state model. (**a**)-(**q**) FH fragments and mutants of FH19–20 binding to amine-coupled recombinant C3d, amine-coupled plasma-derived C3d, and physiologically immobilized C3dg. (**r**) Summary of the affinity constants of FH fragments and mutants for recombinant C3d, plasma-derived C3d and physiologically immobilized C3dg as shown in panels (**a**)-(**q**). (**s**) Antibody (anti-C3c, -iC3b, -C3d) binding to amine-coupled recombinant C3d, amine-coupled plasma-derived C3d, and physiologically immobilized C3dg. Only anti-C3d binding was detected in (i) and (ii). The high response in (iii) corresponds to binding of anti-C3d, the low response to anti-C3c. Binding of anti-iC3b was barely detectable. (**t**) (i) 1 and 10 μM injection of FH15–19 and FH19–20 (for reference) on amine-coupled C3b. The only detectable response corresponds to FH19–20; (ii) and (iii) sensorgram and corresponding K_D fitting for FH18–20 binding to C3b are shown, respectively. The K_D was 9.8±0.4 μM. (**u**)-(**α**) Binding of wild-type FH19–20 and selected mutants to amine-coupled C3d E117A , C3d D122A, C3d E160A, C3d I164A, C3d E117A D122A. (**β**) Binding of wild-type FH19–20 to amine-coupled C3d in the presence of a 20-fold excess of the heparin homologue, Fondaparinux.

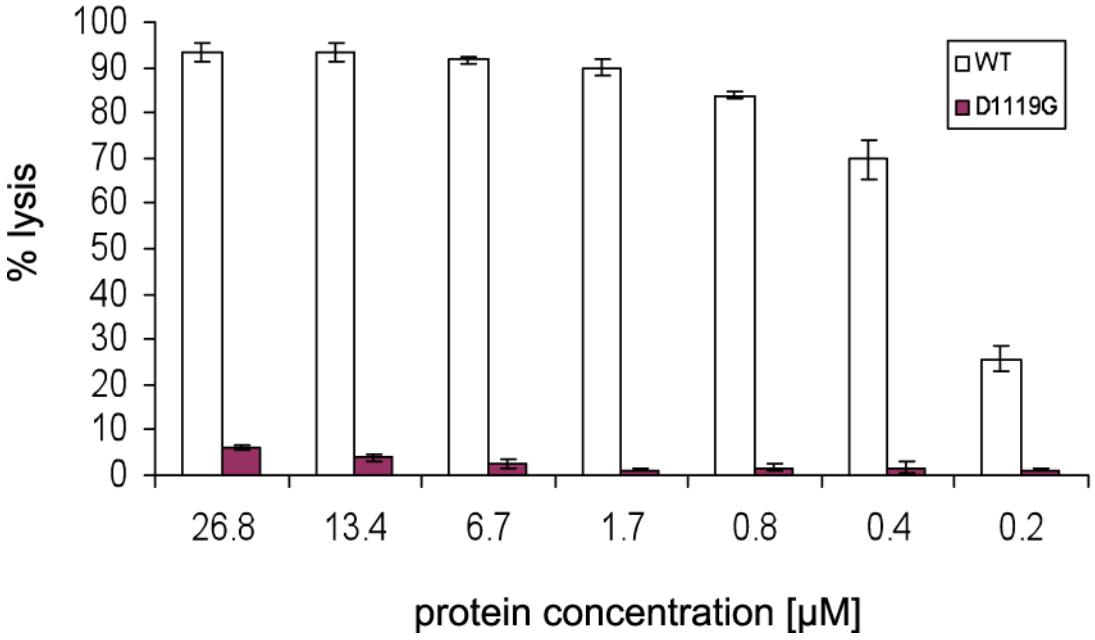

Supplementary Figure 5 Capacity of wild-type and D1119G mutant form of FH19–20 to inhibit FH-mediated protection of sheep erythrocytes from complement-driven cell lysis. Sheep erythrocytes were incubated with varying concentrations of wild-type or D1119G forms of FH19–20 ranging from 0.2 μM to 26.8 μM in the presence of normal human serum (NHS). While wild-type FH19–20 was able to effectively compete with the serum's full-length FH for erythrocyte binding even at low concentrations, the D1119G mutant was found to have no capacity to inhibit FH-mediated protection. Each experiment was repeated four times; standard deviations are shown as error bars.

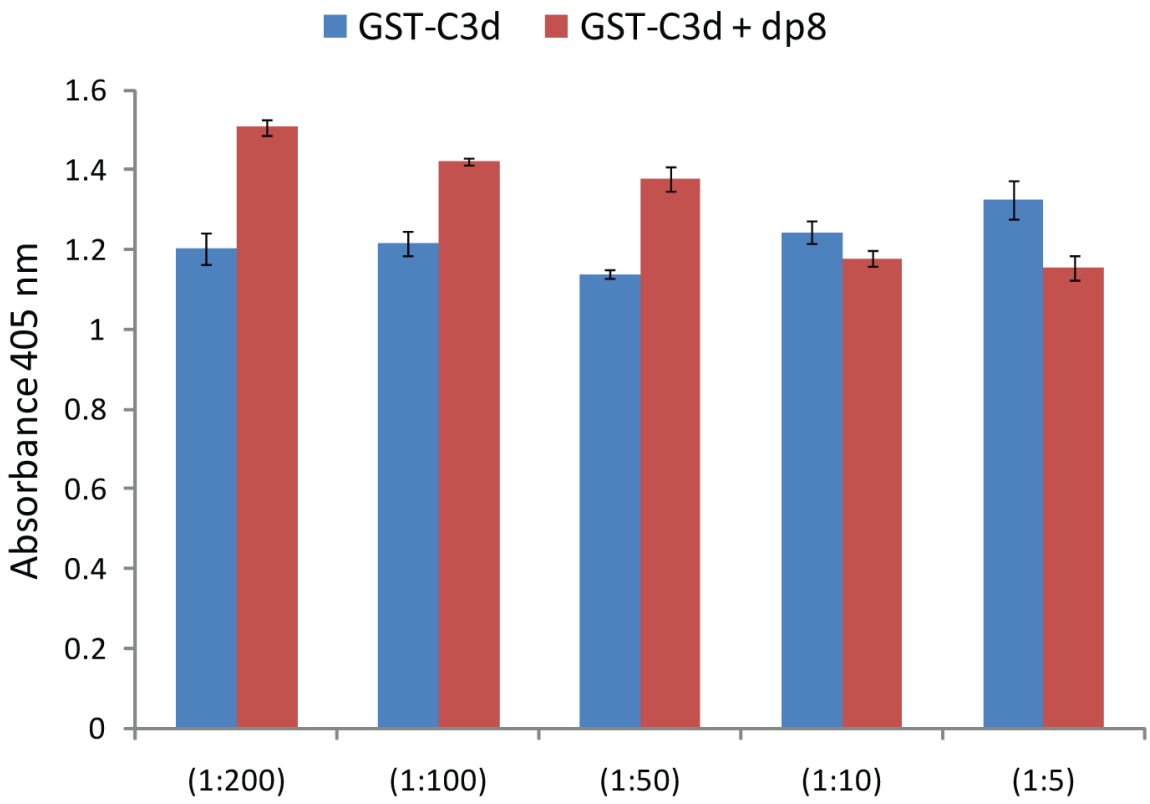

Supplementary Figure 6 Capacity of the octasaccharide fraction of heparin, dp8, to inhibit binding of GST-C3d to platebound FH19–20. Molar excesses of 200-fold to 5-fold of dp8 were found to result in little or no effect on GST-C3d binding (at a concentration of 30 μg/ml), as detected utilizing a horse-radish peroxidase-conjugated anti-GST monoclonal antibody.

(a)

Sample (*MW*, kD^2)	***R_g*, nm**	***D_{max}*, nm**	***V_p*, nm^3**	***MW_{SAXS}*, kD**	**χ_s**
FH 1–4 (30.2)	4.3 ± 0.1	13.8 ± 0.5	46 ± 5	31 ± 3	0.96
FH 8–15 (54.7)	3.5 ± 0.1	12.0 ± 0.5	82 ± 8	54 ± 5	1.04
FH 15–19 (34)	4.5 ± 0.1	14.8 ± 0.5	65 ± 7	43 ± 4	1.04

(b)

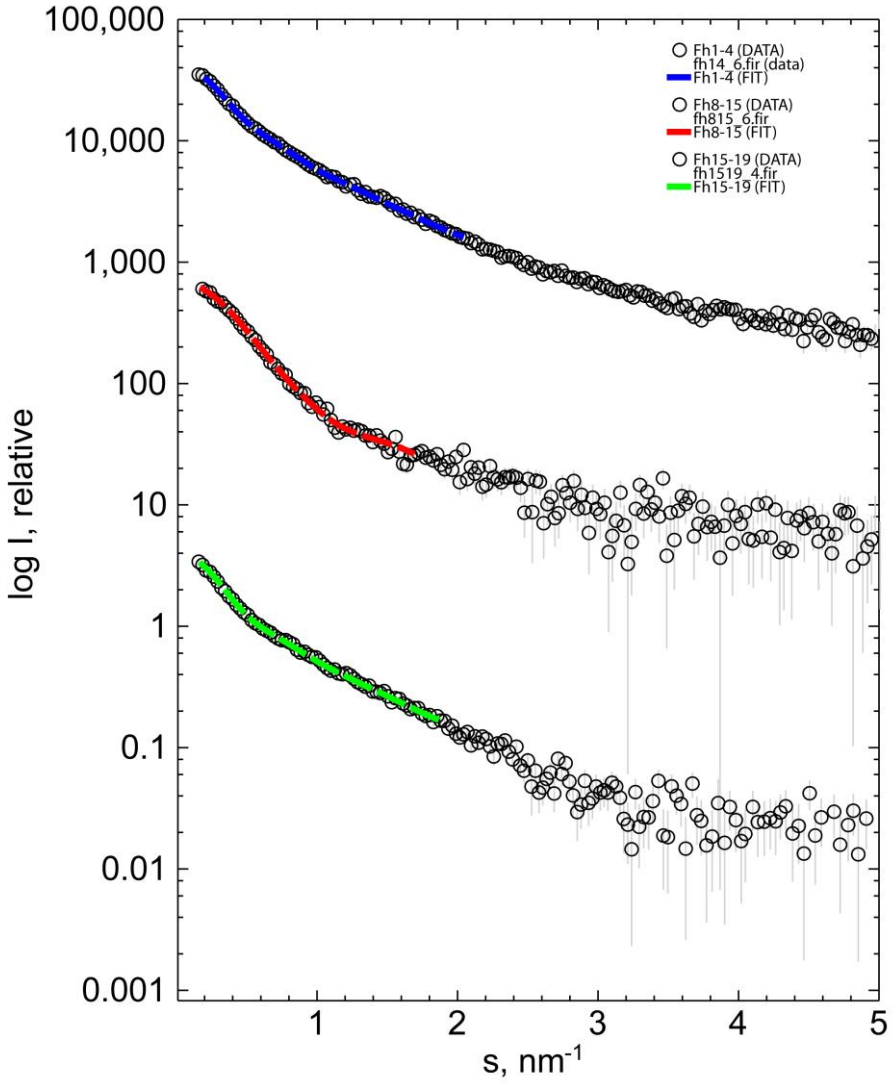

Supplementary Figure 7 (**a**) Overall SAXS parameters: [1] R_g, D_{max}, V_p and MW_{saxs} are the experimentally (SAXS) determined radius of gyration, maximum particle dimension, hydrated particle volume, and molecular weight, respectively. χ_s is the discrepancy between the experimental data and computed scattering curves from the most typical *ab initio* models. [2]Molecular weight calculated from sequence. (**b**) SAXS data and *ab initio* modelling. Scattering curves for FH1–4, FH8–15 and FH15–19. Dotted lines represent fits of the calculated *ab initio* DAMMIF models to the SAXS data (blue: FH1–4, red: FH8–15, green: FH15–19); curves have been arbitrarily displaced along the logarithmic axis for clarity.

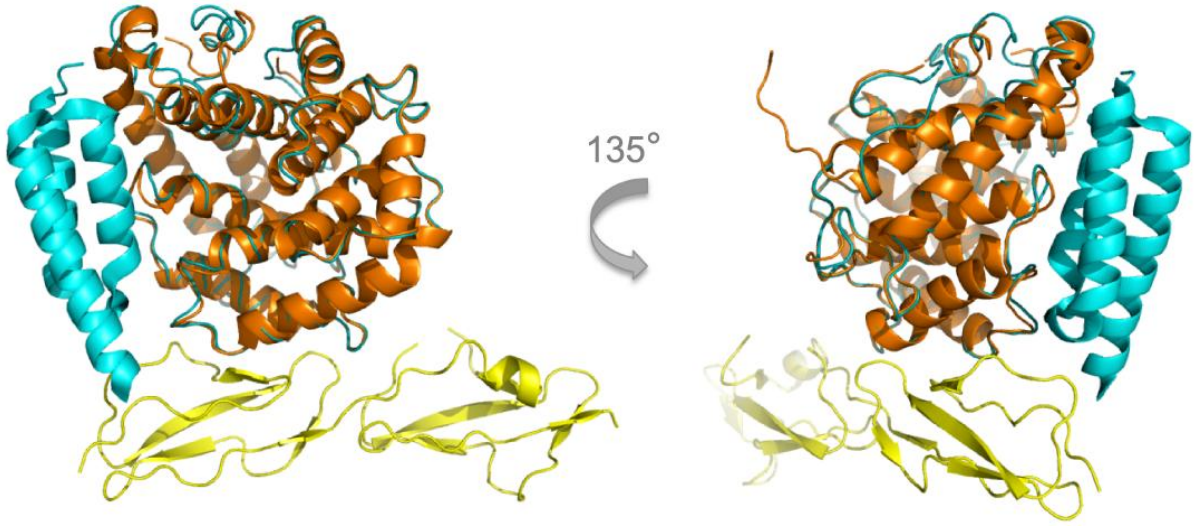

Supplementary Figure 8 Superposition of the C3d:FH19–20 complex on the previously determined structure of the C3-binding domain of the staphylococcal extracellular fibrinogen binding protein (Efb-C) in complex with C3d [7]. The superposition illustrates that the hypervariable loop of FH CCP19 is in close proximity to the N-termini of helices α1 and α3. A recent study has demonstrated that Efb-C has the ability to enhance the binding of the two C-terminal modules of FH (CCP19-20) to C3b [8], but completely blocks the C3b:FH1-4 interaction, due to overlap of the Efb-C and FH1–4 binding sites. The overall effect of Efb-C binding to C3b is to enhance C3b-FH1-20 binding, but with full-length FH exhibiting a less significant increase in binding to that of FH19–20. This has been attributed to the opposing consequences Efb-C binding has on the binding of CCP1-4 and CCP19-20, with CCP1-4 being inhibited, and CCP19-20 being significantly enhanced [8].

(a)

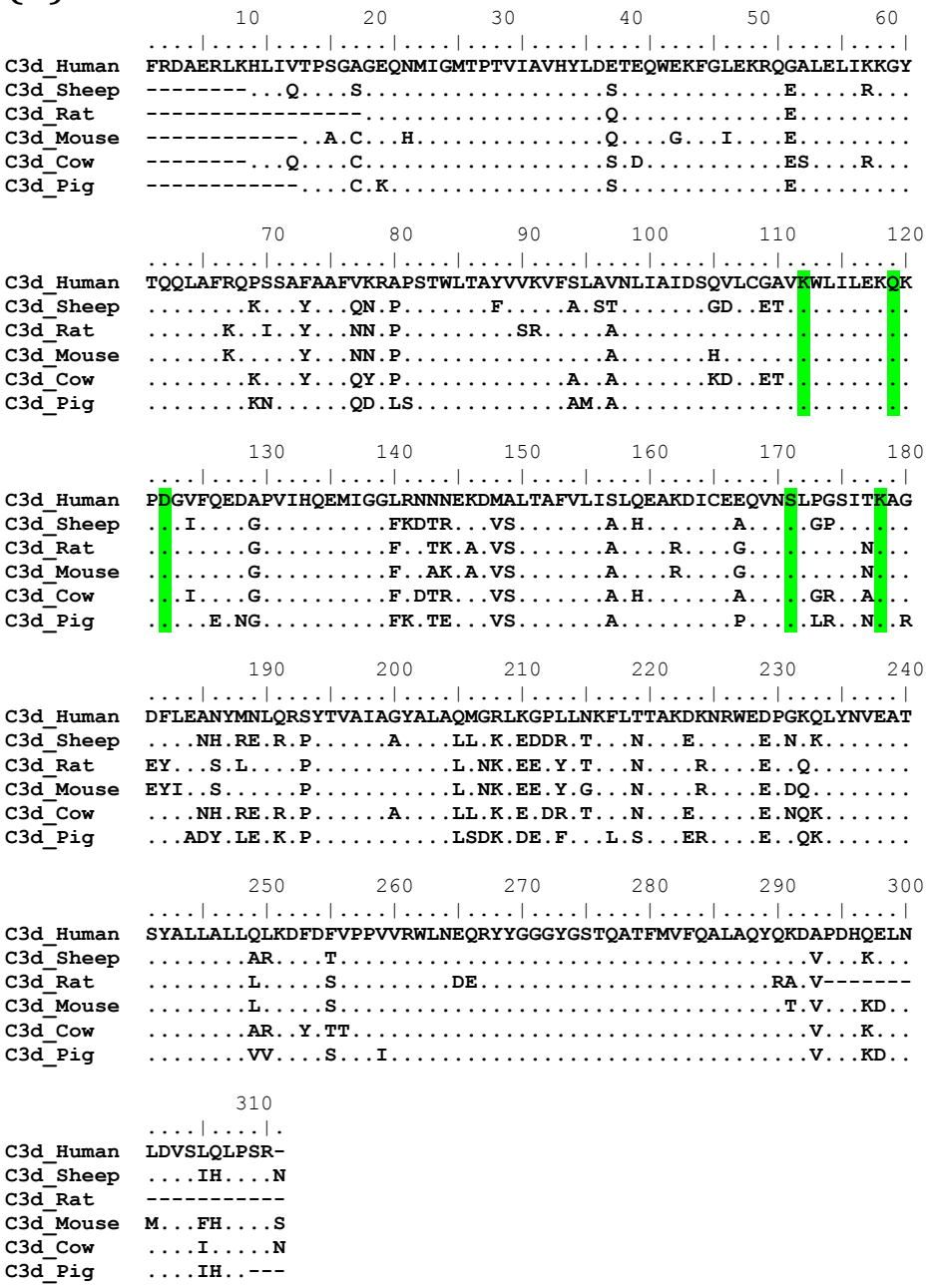
10 20 30 40 50 60
C3d_Human FRDAERLKHLIVTPSGAGEQNMIGMTPTVIAVHYLDETEQWEKFGLEKRQGALELIKKGY
C3d_Sheep --------...Q....S.....S.....E.....R...
C3d_Rat -----------------.....Q.....E.....
C3d_Mouse ------------..A.C...H.....Q....G...I....E.....
C3d_Cow --------...Q....C.....S.D.....ES....R...
C3d_Pig ------------....C.K.....S.....E.....
70 80 90 100 110 120
C3d_Human TQQLAFRQPSSAFAAFVKRAPSTWLTAYVVKVFSLAVNLIAIDSQVLCGAVKWLILEKQK
C3d_Sheep .....K...Y...QN.P.....F.....A.ST.....GD..ET.....
C3d_Rat .....K..I..Y...NN.P.....SR.....A.....
C3d_Mouse .....K.....Y...NN.P.....A.....H.....
C3d_Cow .....K...Y...QY.P.....A..A.....KD..ET.....
C3d_Pig .....KN.....QD.LS.....AM.A.....
130 140 150 160 170 180
C3d_Human PDGVFQEDAPVIHQEMIGGLRNNNEKDMALTAFVLISLQEAKDICEEQVNSLPGSITKAG
C3d_Sheep ...I....G.....FKDTR...VS.....A.H.....A.....GP.....
C3d_Rat .....G.....F..TK.A.VS.....A....R....G.....N...
C3d_Mouse .....G.....F..AK.A.VS.....A....R....G.....N...
C3d_Cow ...I....G.....F.DTR...VS.....A.H.....A.....GR..A...
C3d_Pig .....E.NG.....FK.TE...VS.....A.....P.....LR..N..R
190 200 210 220 230 240
C3d_Human DFLEANYMNLQRSYTVAIAGYALAQMGRLKGPLLNKFLTTAKDKNRWEDPGKQLYNVEAT
C3d_Sheep ....NH.RE.R.P.....A....LL.K.EDDR.T...N...E.....E.N.K.....
C3d_Rat EY...S.L....P.....L.NK.EE.Y.T...N....R....E..Q.....
C3d_Mouse EYI..S.....P.....L.NK.EE.Y.G...N....R....E.DQ.....
C3d_Cow ....NH.RE.R.P.....A....LL.K.E.DR.T...N...E.....E.NQK.....
C3d_Pig ...ADY.LE.K.P.....LSDK.DE.F...L.S...ER....E..QK.....
250 260 270 280 290 300
C3d_Human SYALLALLQLKDFDFVPPVVRWLNEQRYYGGGYGSTQATFMVFQALAQYQKDAPDHQELN
C3d_Sheep .....AR....T.....V...K...
C3d_Rat .....L.....S.....DE.....RA.V-------
C3d_Mouse .....L.....S.....T.V...KD..
C3d_Cow .....AR..Y.TT.....V...K...
C3d_Pig .....VV....S...I.....V...KD..
310
C3d_Human LDVSLQLPSR-
C3d_Sheep ....IH....N
C3d_Rat ----------
C3d_Mouse M...FH....S
C3d_Cow ....I.....N
C3d_Pig ....IH..---

(b)

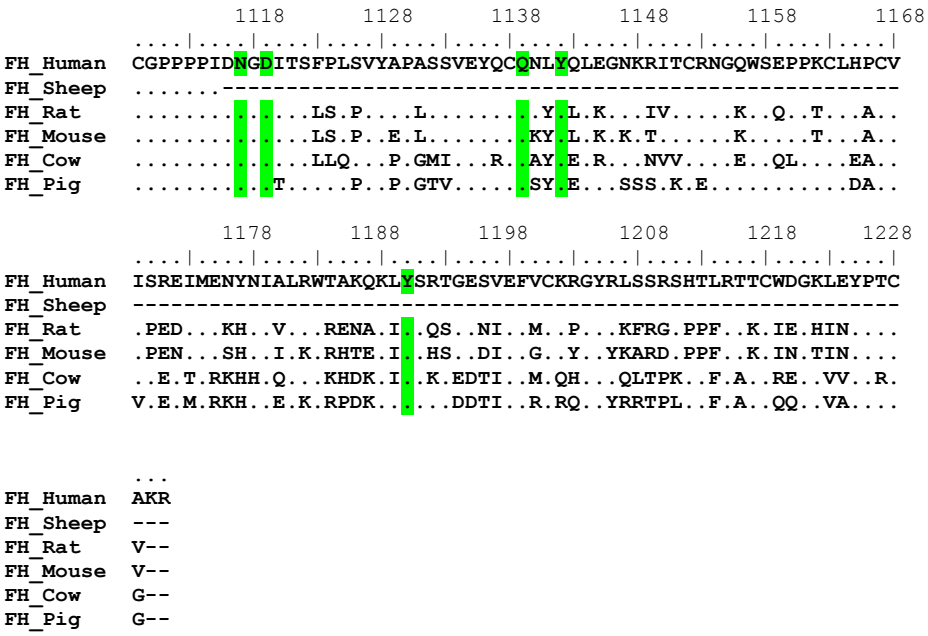

Supplementary Figure 9 (**a**) C3d sequence alignment. Side chains of C3d residues which form hydrogen bonds to FH19–20 are highlighted in green. Accession numbers are as follows; C3d_Human = P01024; C3d_Sheep = ABR24137; C3d_Rat = 9954969; C3d_Mouse = ABD66220; C3d_Cow = AAT76518; C3d_Pig = ADG26759. (**b**) FH19–20 sequence alignment. Side chains of FH residues which form hydrogen bonds to C3d are highlighted in green. FH sequences have been truncated to show only modules 19 and 20. Accession numbers are as follows; FH_Human = CAA68704; FH_Sheep = ADF57191; FH_Rat = NP_569093.2; FH_Mouse = NP_034018.2; FH_Cow = AAI05259.1; FH_Pig = CAC81999.1.

Supplementary Methods

Glycosaminoglycan (GAG) preparation

Bovine lung heparin (Calbiochem, 375093) was digested enzymatically using heparinase I (Grampian Enzymes) and prepared as previously described [9]. The reaction mixture was then freeze-dried and size-fractionated using a 180 x 2.6 cm Bio Gel P-10 (BioRad, 1504144) gel filtration column in 0.2 M ammonium bicarbonate with a flow rate of 0.5 ml/min. The octasaccharide fraction was repeatedly freeze-dried and dissolved in distilled water to remove residual ammonium bicarbonate. The GAG concentration was determined using the absorbance at 232 nm [10].

Preparation of sheep erythrocytes Sheep erythrocytes were obtained from defibrinated sheep blood (TCS Biosciences). 1 ml of blood was transferred to a 15 ml falcon tube and diluted with 10 ml of 20 mM HEPES, 145 mM NaCl, 0.1 % (w/v) gelatin (from pork skin, Fluka) and 10 mM EDTA, pH 7.3 at 25 °C. The cell suspension was mixed gently and then spun for 10 min at 500 X g, at 4 °C. The supernatant and a layer of leucocytes were aspirated off and the procedure was repeated two more times. The wash buffer was then replaced by an identical buffer without EDTA, and the procedure was repeated an additional three times, this time spinning the samples at 1000 X g. Cells were stored at 4 °C for up to one week and immediately before use underwent an additional wash stage in EDTA-free buffer to remove any cellular debris which may have accrued during storage.

Hemolytic Assay Lysis of sheep erythrocytes was carried out using an adaptation of a hemolytic assay described by Sánchez-Corral *et al* [11], which was previously successfully

applied to recombinant FH19–20 [12]. 20 µl of normal human serum (NHS) were mixed with 1.25 µl of 0.1 M MgEGTA (1:1 $MgCl_2$ and ethylene glycol-bis(2-aminoethyl)-N,N,N',N'-tetraacetic acid), 2.5 µl of sheep erythrocytes stock solution and 1.25 µl of buffer (20 mM HEPES, 145 mM NaCl, 5 mM MgEGTA, 0.1% (w/v) gelatin, pH 7.3 at 25 °C). The concentration of erythrocytes in the cell stock was adjusted so that it gave an OD reading at 412 nm ($A_{412\ nm}$) of 0.5-0.6 if completely lysed in distilled water. This value was subsequently used as the 100% lysis value during analysis of the results. To the 25 µl solution containing NHS and erythrocytes an additional 25 µl of varying concentrations of wild-type FH19–20 or the D1119G mutant protein, prepared in the aforementioned buffer, but without gelatine, was added. The 50 µl reaction mixture was incubated at 37 °C for 20 min and quenched by the addition of 150 µl cold quenching buffer (20 mM HEPES, 145 mM NaCl, 5 mM EDTA, pH 7.3). The cells were then centrifuged for five minutes at 1500 X g, 4 °C, in a 96 well plate. 100 µl of supernatant from each condition was transferred to a fresh 96 well plate, which was read at $A_{412\ nm}$. Each experiment was repeated four times. As a negative control the same reaction mixture was prepared, incubated and quenched using serum which had been heat-inactivated at 56 °C for 30 min [13]. The percentage lysis was determined by subtracting the $A_{412\ nm}$ of the background lysis control and dividing by the maximum lysis in water.

GST-C3d Production

Cultures of *E. coli* transformed with PGEX-6P-1 plasmid (GE Healthcare) additionally containing the C3d insert were grown at 37 °C until an A_{600} of 0.3 was obtained. Cultures were induced with 0.3 mM IPTG overnight at 20 °C prior to harvesting by centrifugation. Harvested pellets were resuspended in 25 mM Tris, pH 8.0, 0.5 M NaCl, 1 mM EDTA, 1 mM DTT and lysed by sonication. After centrifugation, the clarified lysate

was applied to a 5 ml GSTrap FF column utilizing an AKTApurifier liquid chromatography device (GEHealthcare). Subsequent to column loading, the GST-tagged C3d was eluted from the column utilizing an elution buffer containing 10 mM reduced glutathione (50 mM Tris-HCl, 10 mM reduced glutathione, pH 8.0). The resulting eluent was concentrated using a Vivaspin 20 centrifugal concentration device (30 KDa MWCO), and then purified on a Hiprep S200 16/60 Sephacryl HR size exclusion column in PBS (PBS: 4.8 mM $MgCl_2$, 2.7 mM KCl, 1.5 mM KH_2PO_4, 136.8 mM NaCl, 8.1 mM Na_2HPO_4, pH 7.4).

GST-C3d:FH19–20:dp8 Competition Assay

Plates were coated overnight at 4 °C by incubation with FH19–20 (10 μg/ml) in 50 mM sodium bicarbonate buffer (pH 8.8) and then blocked with 1% BSA in PBS (pH 7.4) for 1 hour at room temperature. Plates were then washed three times with PBS–Tween 20 (0.05%). Recombinant wild-type GST-C3d (30 μg/ml) was added to half of the FH-coated wells to act as a positive control. To the other half of the C3d-coated wells, recombinant wild-type GST-C3d (30 μg/ml) additionally containing the octasaccharide fraction of heparin, dp8, at concentrations ranging from a 5:1 molar excess of dp8:GST-C3d up to a 200:1 molar excess of dp8:GST-C3d. After a 1-hour incubation period, the plates were washed, and GST-C3d binding was then detected with commercially available HRP-conjugated anti-GST mAb (GE-Healthcare).

Crystallization of C3d:FH19–20 at pH 7.0 Additional crystals of the C3d:FH19–20 complex were also grown in hanging drops in which the well solution comprised 0.1 M Na HEPES, pH 7.0, 15% w/v PEG 20000. Crystals were flash frozen in liquid nitrogen after soaking in cryoprotectant solutions additionally containing 10% glycerol.

Structure determination C3d complexed with FH19–20 (C3d:FH19–20) was determined at 2.1 Å resolution (**see Table 1 for data collection and refinement statistics**). Crystals were triclinic (space group P1) and contained 3 monomers of both C3d and FH19–20 in the unit cell. All monomers were very similar, C3d monomers had an average RMSD of 0.33 Å (range 0.44 - 0.26 Å) for all C^{α} atoms of residues 18–294 and FH monomers had an average RMSD of 0.87 Å (range 0.66–1.127 Å) for all C^{α} atoms of residues 1107–1230. The physiologically relevant complex is form between chain B (C3d) and chain F (FH). Clearly interpretable electron density was observed for all residues forming the C3d:FH19–20 interface. Lower resolution data (3.5 Å) were also obtained for crystals grown at pH7.0 as described above. Data for these crystals were collected and processed as set out in the **ONLINE METHODS**.

Surface plasmon resonance Surface plasmon resonance binding studies were carried out utilizing a Biacore T100 device. All analyte injections were carried out in duplicate and duplicate sensorgrams of dummy-surface responses are plotted throughout.

Binding to recombinant C3d, plasma-derived C3d and physiologically immobilized C3dg.

A total of 500 and 1480 response units of wild-type recombinant C3d purified as described above or commercially available (Complement Technologies Inc) were independently amine-coupled to a CM5 sensor chip (carboxymethylated dextran surface; Biacore International) in flow cells 2 and 3 (Fc2 and Fc3), respectively. In addition, in flow cell 4 (Fc4) physiologically-immobilized, analogous C3dg was coated to a CM5 sensor chip by first amine coupling a total of 100 RU of commercially available human C3b (Complement Technologies Inc) to the chip surface. C3bBb convertase complexes were then generated by injection of a mixture of complement Factor B

(0.2μM) and complement Factor D (0.02 μM) over Fc4. Subsequent injection of C3 over the surface of Fc4 then resulted in the deposition of C3b immobilized to the chip surface through the native thioester group. A total of 1320 RU of C3b were immobilized on Fc4 in this way. C3b was then cleaved to its C3dg form by application of a mix of complement receptor type 1 and complement Factor I over Fc4, resulting in deposited C3dg immobilized on the flow cell surface in a way analogous to that of physiologically-deposited C3dg on the surface of mammalian cells. The running and sample buffer for this physiological immobilization comprised 10 mM HEPES, 150 mM NaCl, 0.005% v/v P20, pH 7.4 (HBS-P) and substituted with 1mM $MgCl_2$.

A total of 200 μl of the wild-type or mutant forms of FH at the concentrations indicated in the figure legend were passed over the flow cells (Fc1-4) at flow rate of 30 μl/min, at 25 °C. The running and sample buffer consisted of 10 mM HEPES, 150 mM NaCl, 3 mM EDTA 0.005% v/v P20, pH7.4 (HBP-EP). A sample contact time of 90 seconds was found to be sufficient to achieve steady-state conditions and was followed by a dissociation time of 360 seconds with HBS-EP as running buffer. Between sample injections the surfaces were regenerated by one injection of 1 M NaCl for contact times of 30 seconds. Data were processed using Biacore T100 evaluation software version 2.0. Reporter points for affinity measurements were set to 2 seconds before injection began and 2 seconds before the injection period finished. Dissociation constants were calculated by fitting steady-state binding levels derived from the background-subtracted traces to a one-to-one binding steady-state model.

After flowing all analyte protein constructs over the sensor chip surfaces, monoclonal antibodies that recognize C3c (clone name: 013E-498.2.3), iC3b (neoepitope) (013III-1.1.6) and C3d (053A-1149.3.1.4) (all murine anti-human at a concentration of 10μg/ml; Quidel) were employed to probe the sensor surfaces.

Analysis of FH15-19 and FH18-20 binding to C3b by surface plasmon resonance.

Plasma-derived C3b was immobilized on CM5 chip via amine coupling (1860 RUs). A concentration series of FH18-20 was flown over the sensor surfaces in HBS-EP buffer and dissociation constants were calculated as described above. FH19–20 and FH15–19 were analyzed for C3b binding at concentrations of 1 and 10 μM.

Analysis of mutant C3d binding by surface plasmon resonance

The recombinant C3d mutants E117A, D122A, E117A D122A, E160A and I164A were immobilized on CM5 chip via amine coupling (650 RUs, 680 RUs, 560 RUs, 670 RUs and 630 RUs, respectively). Concentration series of wild-type and R1182S, L1189F, L1189R and R1915Q mutant versions of FH19–20 were flown over the sensor surfaces for the E117A, D122A and E160A mutants, in HBS-EP buffer, and wild-type FH19–20 only, was flown over the sensor surfaces for the E117A D122A and I164A mutants. Dissociation constants were calculated as described above.

GAG:FH19–20:C3d Competition Assay by surface plasmon resonance

530 RU of recombinant C3d were immobilised on a CM5 sensor-chip surface using standard amine coupling. A concentration series of FH19–20 and of FH19–20 in the presence of a 20-fold excess of the pentasaccharide heparin analogue, Fondaparinux, were probed for C3d-binding in HBS-EP buffer. Dissociation constants were calculated as previously described.

NMR Spectroscopy of the C3d:FH19–20 complex and mapping the FH19–20-GAG binding sites All spectra of the FH19–20-interactions were acquired at 800 MHz as stated in the **ONLINE METHODS** section. An NMR sample of a C3d:^{15}N-labelled FH19–20 complex was prepared in a 3 mm NMR tube and contained 40 μM C3d and 25 μM

^{15}N-FH19–20 in 20 mM potassium phosphate, pH 7.0, 10 % D_2O. [$^1H^{15}N$]-HSQC spectra were acquired over 32 scans using 92 and 34 ms acquisition times in the directly and indirectly detected dimensions. Spectra were zero filled prior to Fourier transformation.

The titration of ^{15}N-FH19–20 with heparin octasaccharide, dp8, was done on a 27 μM sample in the same buffer. FH19–20:dp8 molecular ratios were 1:0, 1:0.5, 1:1.1, 1:2.1, 1:4.3 and 1:8.5. 16 scans were acquired using the parameters given above. To the sample of the C3d:^{15}N-FH19–20 complex, dp8 was added to 1:0, 1:0.6, 1:7.9 and 1:15.0 equivalents (molecular ratios of FH19–20:dp8) and [$^1H^{15}N$]HSQC spectra were recorded for every titration point.

Small-angle X-ray scattering Synchrotron radiation X-ray scattering data were collected on the X33 beamline of the EMBL (DESY, Hamburg) [14,15], using a PILATUS 1M pixel array detector (Dectris, Switzerland) and four frames of 30 seconds exposure time. Solutions of FH constructs were measured at 10 °C in 50 mM potassium phosphate buffer, pH 7.4, at protein concentrations of 0.9 and 2.7 mg/ml^{-1} (FH1–4), 0.5, 0.9 and 2.2 mg/ml^{-1} (FH8–15), and 1.3, 2.7, and 5.3 mg/ml^{-1} (FH15–19). The sample-to-detector distance was 2.7 m, covering a range of momentum transfer $0.1 < s < 6.0$ nm^{-1} ($s = 4\pi\sin\theta/\lambda$, where 2θ is the scattering angle, and $\lambda = 0.15$ nm is the X-ray wavelength). For FH8–15 and FH15–19, radiation damage was observed as a significant increase in the intensities of low-angle data after the second 30-s exposure. For this data only the first frames were used for data analysis. Data from the detector were normalized to the incident beam intensity, averaged and the scattering of buffer solutions subtracted. The difference curves were scaled for solute concentration. All data manipulations were performed using the *PRIMUS* software package [16].

The forward scattering $I(0)$ and radius of gyration (R_g) were determined from Guinier analysis [17], assuming that at very small angles ($s < 1.3/R_g$) the intensity is given by $I(s) = I(0)\exp(-(sR_g)^2/3)$. These parameters were also estimated from the full scattering curves using the indirect Fourier transform method implemented in the program GNOM [18], along with the distance-distribution function *p(r)* and the maximum particle dimensions D_{max}. Molecular weights (MWs) of solutes were estimated from SAXS data by comparing extrapolated forward scattering with that of a reference solution of bovine serum albumin.

Due to the uncertainty in MW estimation from SAXS data that results from uncertainty in the measured protein concentrations, an excluded volume of the solutes was determined from the *ab initio* modelling program DAMMIF [19]. This estimation is independent of protein concentration and can be obtained in an automated fashion with minimal user bias. For globular proteins, this hydrated particle volume in nm^3 is approximately 1.5 to 2 times the MW in kDa.

***Ab initio* shape determination and molecular modeling** Low-resolution shape envelopes for the FH constructs were determined using the *ab initio* bead-modelling program DAMMIF [19]. DAMMIF represents the particle as a collection of *M* (>> 1) densely packed beads inside an adaptable and loosely constrained search volume compatible with the experimentally determined R_g. Each bead is randomly assigned to solvent (index = 0) or solute (index = 1), and the particle structure in solution described by a binary string of length M. Disconnected strings of beads are rejected and the scattering amplitudes calculated. Simulated annealing is then used to search for a compact model that minimizes the discrepancy:

$$x^2 = \sum_k \frac{1}{N-1} \sum_j \left[\frac{I_{exp}(S_j) - cI_{calc}(S_j)}{\sigma(S_j)} \right]$$

where N is the number of experimental points, $I_{exp}(s_j)$ and $I_{calc}(s_j)$ are the experimental and calculated intensities, c is a scaling factor and $\sigma(s_j)$ is the experimental error at the momentum transfer s_j.

The results of multiple DAMMIF reconstructions were compared using the alignment program SUPCOMB [20] to determine the most representative (typical) model from each of the *ab initio* methods. Averaged DAMMIF models were also determined using the programs DAMAVER [16] and these models adjusted such that they agree with the experimentally determined excluded volume using the program DAMFILT [21].

Supplementary References

1. Krissinel, E. & Henrick, K. Inference of macromolecular assemblies from crystalline state. *J. Mol. Biol.* 372, 774-97 (2007).
2. Ferreira, V.P. et al. The Binding of Factor H to a Complex of Physiological Polyanions and C3b on Cells Is Impaired in Atypical Hemolytic Uremic Syndrome. *J. Immunol.* 182, 7009-7018 (2009).
3. Wu, J. et al. Structure of complement fragment C3b-factor H and implications for host protection by complement regulators. *Nat. Immunol.* 10, 728-33 (2009).
4. Lehtinen, M.J., Rops, A.L., Isenman, D.E., van der Vlag, J. & Jokiranta, T.S. Mutations of factor H impair regulation of surface-bound C3b by three mechanisms in atypical hemolytic uremic syndrome. *J. Biol. Chem.* 284, 15650-8 (2009).
5. Janssen, B.J., Christodoulidou, A., McCarthy, A., Lambris, J.D. & Gros, P. Structure of C3b reveals conformational changes that underlie complement activity. *Nature* 444, 213-6 (2006).
6. Wiesmann, C. et al. Structure of C3b in complex with CRIg gives insights into regulation of complement activation. *Nature* 444, 217-20 (2006).
7. Hammel, M. et al. A structural basis for complement inhibition by Staphylococcus aureus. *Nat. Immunol.* 8, 430-7 (2007).
8. Chen, H. et al. Allosteric inhibition of complement function by a staphylococcal immune evasion protein. *Proc. Natl. Acad. Sci. U S A* In Press(2010).
9. Deakin, J.A., Blaum, B.S., Gallagher, J.T., Uhrin, D. & Lyon, M. The binding properties of minimal oligosaccharides reveal a common heparan sulfate/dermatan sulfate-binding site in hepatocyte growth factor/scatter factor that can accommodate a wide variety of sulfation patterns. *J. Biol. Chem.* 284, 6311-21 (2009).

10. Linhardt, R.J. et al. Mapping and quantification of the major oligosaccharide components of heparin. *Biochem. J.* 254, 781-7 (1988).
11. Sanchez-Corral, P., Gonzalez-Rubio, C., de Cordoba, S.R. & Lopez-Trascasa, M. Functional analysis in serum from atypical Hemolytic Uremic Syndrome patients reveals impaired protection of host cells associated with mutations in factor H. *Mol. Immunol.* 41, 81-84 (2004).
12. Ferreira, V.P., Herbert, A.P., Hocking, H.G., Barlow, P.N. & Pangburn, M.K. Critical role of the C-terminal domains of factor H in regulating complement activation at cell surfaces. *J. Immunol.* 177, 6308-16 (2006).
13. Kavanagh, D. et al. The decay accelerating factor mutation I197V found in hemolytic uraemic syndrome does not impair complement regulation. *Mol. Immunol.* 44, 3162-3167 (2007).
14. Koch, M.H.J. & Bordas, J. X-ray-diffraction and scattering on disordered-systems using synchotron radiation *Nucl. Instrum. Methods Phys. Res.* 208, 461-469 (1983).
15. Roessle, M.W. et al. Upgrade of the small-angle X-ray scattering beamline X33 at the European Molecular Biology Laboratory, Hamburg. *J. Appl. Crystallogr.* 40, S190-S194 (2007).
16. Konarev, P.V., Volkov, V.V., Sokolova, A.V., Koch, M.H.J. & Svergun, D.I. PRIMUS: a Windows PC-based system for small-angle scattering data analysis. *J. Appl. Crystallogr.* 36, 1277-1282 (2003).
17. Guinier, A. La diffraction des rayons X aux tres petits angles; application a l'etude de phenomenes ultramicroscopiques. *Ann. Phys. (Paris)* 12, 161-237 (1939).
18. Svergun, D.I. Determination of the regularization parameter in indirect-transform methods using perceptual criteria. *J. Appl. Crystallogr.* 25, 495-503 (1992).
19. Franke, D. & Svergun, D.I. DAMMIF, a program for rapid ab-initio shape determination in small-angle scattering. *J. Appl. Crystallogr.* 42, 342-346 (2009).
20. Kozin, M.B. & Svergun, D.I. Automated matching of high- and low-resolution structural models. *J. Appl. Crystallogr.* 34, 33-41 (2001).
21. Volkov, V.V. & Svergun, D.I. Uniqueness of ab initio shape determination in small-angle scattering. *J. Appl. Crystallogr.* 36, 860-864 (2003).